



Global Earth Observation for integrated water resource assessment

Report on the current state-of-the-art Water Resources Reanalysis

Deliverable No: D.5.1 – Report on the current state-of-the-art Water Resources
Reanalysis (WRR1-tier 1)

Ref.: WP5 - Task 5.1

Date: March 2015





Deliverable Title	D.5.1 – Report on the current state-of-the-art Water Resources Reanalysis
Filename	E2O_D51_v5.docx
Authors	Emanuel Dutra (ECMWF)
Contributors	Gianpaolo Balsamo (ECMWF) Jean-Christophe Calvet (Meteo-France) Marie Minvielle (Meteo-France) Stephanie Eisner (Uni Kassel) Gabriel Fink (Uni Kassel) Stefanie Pessenteiner (Uni Utrecht) René Orth (ETH) Sophia Burke (Ambiotek) Albert van Dijk (CSIRO) Jan Polcher (CNRS) Hylke Beck (JRC) Alberto Martinez de La Torre (CEH)
Reviewers	Geert, Sterk (UU)
Date	31/03/2015

Prepared under contract from the European Commission
 Grant Agreement No. 603608
 Directorate-General for Research & Innovation (DG Research), Collaborative project, FP7-ENV-2013-two-stage

Start of the project: 01/01/2014
 Duration: 48 months
 Project coordinator: Stichting Deltares, NL

Dissemination level

<input checked="" type="checkbox"/>	PU	Public
<input type="checkbox"/>	PP	Restricted to other programme participants (including the Commission Services)
<input type="checkbox"/>	RE	Restricted to a group specified by the consortium (including the Commission Services)
<input type="checkbox"/>	CO	Confidential, only for members of the consortium (including the Commission Services)

Deliverable status version control

Version	Date	Author	Reviewer	Singed-off by
0.0	3/12/2014	Emanuel Dutra	-	-



1.0	27/01/2015	Emanuel, Dutra (ECMWF)	-	-
2.0	13/02/2015	Emanuel Dutra		
3.0	01/02/2015	Emanuel Dutra		
4.0	16/02/2015	Emanuel Dutra	Geert Sterk	
5.0	30/03/2015	Emanuel Dutra		



Table of Contents

1	Executive Summary.....	1
2	Introduction.....	2
3	Modelling protocol	4
3.1	Meteorological forcing	4
3.2	Simulations setup.....	6
3.3	Models output.....	6
4	Modelling systems.....	10
4.1	HTESSEL-CaMa	13
4.2	JULES	14
4.3	LISFLOOD	16
4.4	ORCHIDEE	17
4.5	PCR-GLOBWB.....	18
4.6	SURFEX-TRIP	20
4.7	WaterWorld	22
4.8	SWBM	23
4.9	W3RA.....	24
4.10	WaterGAP3	25
5	Data.....	27
5.1	Data access	27
5.2	Metadata and quality control	28
6	Inter-comparison.....	30
6.1	Multi-model.....	30
6.2	Verification examples	31
7	Summary	34
8	Appendix A – Data server access example	35
9	Appendix B - Figures	38
10	References	50

List of Figure

Figure 2.1: Overview of the water resources reanalysis time line production, and connection with other work packages.....	2
Figure 4.1: HTESSEL surface and subsurface discretization scheme.....	13
Figure 4.2: Jules model concept.....	15
Figure 4.3: Overview of the LISFLOOD model. P = precipitation; Int = interception; EWint = evaporation of intercepted water; Dint = leaf drainage; ESa = evaporation from soil surface; Ta = transpiration (water uptake by plant roots); INFact = infiltration; Rs = surf ace runoff; D1,2 = drainage from top- to subsoil; D2,gw = drainage from subsoil to upper groundwater zone; Dpref,gw = preferential flow to upper groundwater zone; Duz,lz = drainage from upper to lower groundwater zone; Quz = outflow from upper groundwater zone; Ql = outflow from lower groundwater zone; Dloss = loss from lower groundwater zone. Note that snowmelt is not included in the figure (even though it is simulated by the model; from (Van Der Knijff et al. 2008).	16
Figure 4.4: ORCHIDEE river routing scheme. The hydrology module computes the partitioning of precipitation (P) into infiltration (I) and surface runoff (R) and then into evapotranspiration (ET) and subsurface runoff (D) for each grid box.....	18
Figure 4.5: PCR-GLOBWB model concept.	19
Figure 4.6: Schematic representation of the ISBA soil hydrological and thermal column for four soil/vegetation types. The soil temperature, T, and moisture, w, nodes are collocated. To extend the temperature profile up to a depth of 12 m, the soil water content is extrapolated to each deeper nodes.	21
Figure 4.7: Schematic of WaterWorld.....	23
Figure 6.1: Multi-model mean (left) and standard deviation (right) of northern hemisphere winter evaporation.....	30
Figure 6.2: Multi-model mean (left) and standard deviation (right) of northern hemisphere winter Runoff.....	30
Figure 6.3: Multi-model mean (left) and standard deviation (right) of northern hemisphere winter SWE. Values above 500 mm (both for the mean and standard deviation) are masked to screen Greenland and Antarctica.	31
Figure 6.4: Multi-model mean (left) and standard deviation (right) of northern hemisphere winter RootMoist.	31
Figure 6.5: Multi-model mean (left) and standard deviation (right) of northern hemisphere winter TotMoist.....	31
Figure 6.6: Mean northern hemisphere winter snow cover fraction in the IMS dataset (top left) compared with the multi-model (MM) mean (top right) and the mean difference between MM-IMS (bottom left) and the MM standard deviation (bottom right).....	32
Figure 6.7: Climatological comparison of observed Δ TWS (mean GRACE product, left column) and simulated with SURFEX (center) for DJF, MAM, JJA and SON over the 2002-2012 period. The spatial correlation between GRACE and SURFEX climatologies are indicated for each season on the SURFEX maps. Right column, the zonal average of Δ TWS for GRACE (black line) and SURFEX (red).....	33
Figure 9.1: Water balance residual for each modelling system. The residual is calculated as the sum of the water fluxes plus the storage term changes between 1th January 1979 and the 31th December 2012. Residuals above +/- 0.432 mm/day are assumed to be above the data precision.....	38
Figure 9.2: Statistics of the Precip (mm day ⁻¹) simulations derived from the monthly means: (left) temporal and spatial minimum; (center) temporal and spatial maximum (right) temporal and spatial mean, with the error bars denoting the spatial standard deviation of the temporal mean. The red symbol indicates that the simulation for a particular model is not available.....	39
Figure 9.3: As Figure 9.2 but for Evap (mm day ⁻¹).	39

Figure 9.4: As Figure 9.2 but for Runoff (mm day⁻¹)..... 39

Figure 9.5: As Figure 9.2 but for PotEvap (mm day⁻¹). 40

Figure 9.6: As Figure 9.2 but for RivOut (m³ s⁻¹). 40

Figure 9.7: As Figure 9.2 but for the SurfMoist (kg m⁻²). 40

Figure 9.8: As Figure 9.2 but for the RootMoist (kg m⁻²). 41

Figure 9.9: As Figure 9.2 but for the TotMoist (kg m⁻²). 41

Figure 9.10: As Figure 9.2 but GroundMoist (kg m⁻²)..... 41

Figure 9.11: As Figure 9.2 but for the SWE (kg m⁻²). 42

Figure 9.12: Mean northern hemisphere winter evaporation in each model 43

Figure 9.13: Mean northern hemisphere winter runoff in each model. 44

Figure 9.14: Mean northern hemisphere winter SWE in each model. 45

Figure 9.15: Mean northern hemisphere winter RootMoist in each model..... 46

Figure 9.16: Mean northern hemisphere winter TotMoist in each model. 47

Figure 9.17: Each line contains a specific model mean northern hemisphere winter simulation of snow cover fraction (left) and the mean difference with the IMS dataset (right)..... 48

Figure 9.18: As Figure 9.17 for the remaining models. 49

List of Tables

Table 3.1: Overview of the meteorological forcing, and the correction applied to the original ERA-Interim during the WFDEI processing..... 4

Table 3.2: Institution identifiers in the model outputs..... 7

Table 3.3: List of output variables and conventions 7

Table 4.1: Modelling systems details 11

Table 4.2: Overview of model parameters used by SWBM..... 23

Table 5.1: Overview of daily simulations (and fixed fields) available in the data server. url and dap contain the direct http download link and the OPENDaP link (remove “.html” for applications access), respectively and NA when the variable is not available. 27

1 Executive Summary

This report describes the first water resources reanalysis (WRR-tier1) produced by 8 project partners and 2 external partners. The report contains a description of the modelling protocol, the modelling systems and the data access and quality control performed. The modelling systems include four land surface models, 5 global hydrological models and a simple water balance model. This first version of the WRR is based on the current modelling systems of each partner forced with a state-of-the-art atmospheric reanalysis. The 9 modelling systems simulations are available in the data server, and the meta-data and overall quality of the dataset and accessibility has been verified to a general standard.

This first release is meant to set a benchmark dataset for future testing of the enhanced reanalysis in tier 2 and to enable the WP3-WP4-WP6 interactions. This report only provides a descriptive document to serve and enable the work of the remaining project work packages and is associated with the milestone MS6 (WRR tier 1 available for other work packages).

2 Introduction

The earth2observe project aims to develop a global water resources re-analysis based on state-of-the-art meteorological re-analysis, improved with earth observations and extended with output from hydrological and land surface models that should be off value for multi-scale water resources assessments and research projects. The modelling activity is concentrated in work-package 5, with the main objectives: (1) generate a first release (or tier 1) reanalysis of the global water cycle (in this report); (2) Investigate the value of earth observations to improve the representation of hydrological processes and enhance the quality of the land data assimilation systems; (3) characterize the uncertainties of an advances reanalysis (tier 2), which builds upon verification, data assimilation and model improvements; and (4) generate an ensemble-bases advances global water reanalysis with associated error estimates.

Multi-model reanalysis of the state of the surface water storage and fluxes provide an ensemble that is not dependent on a single model. This is generally superior to the results of any individual model, and as good as or better than the best model at each point and time (Dirmeyer et al. 2006). Considering the significant uncertainties in modelling the different components of the surface water cycle a multi-model approach can consider the inter-model uncertainties that can be used in downstream applications of water resources.

The multi-model approach has been a recurrent approach in several international projects (e.g. GSWP2 (Dirmeyer et al. 2006), EU-WATCH (Harding et al. 2011), and in Earth2Observe we start by generating a first version of the water resource reanalysis (tier1, WRR). This first version is based on a set of different land surface and hydrological models simulations with their current modelling system with a controlled modelling protocol. This will provide a benchmark reanalysis enabling to evaluate improvements within the project lifetime. The verification phase 1 in WP4 will establish the link with the multi-model output, and gather verification results from the remaining work packages (see Figure 2.1 for an overview of the water resources reanalysis time line production).

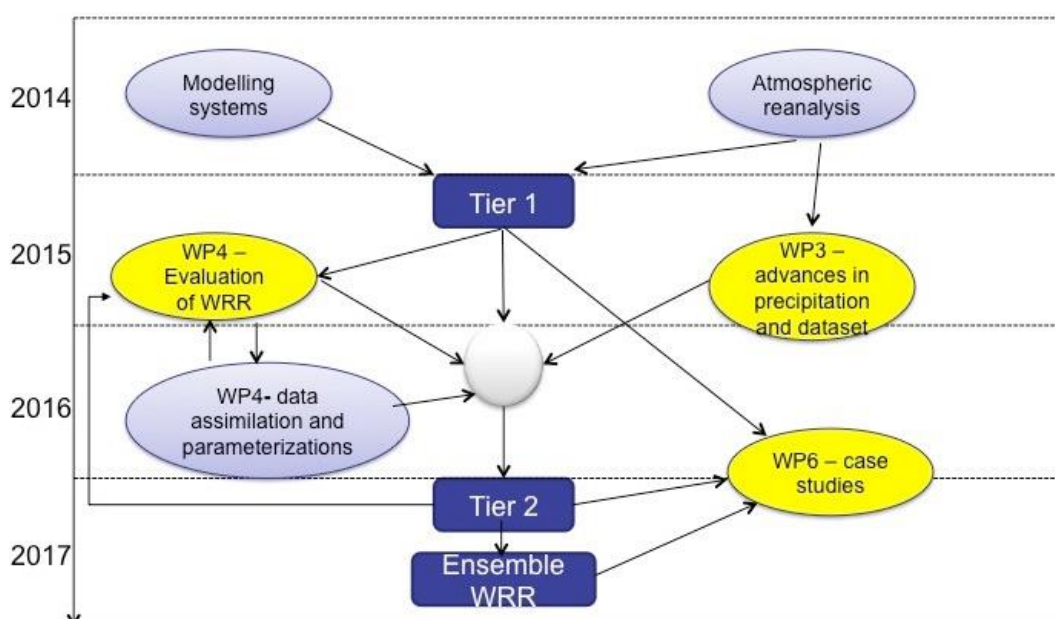


Figure 2.1: Overview of the water resources reanalysis time line production, and connection with other work packages.

This report serves as a baseline for the water resources reanalysis defining the general modelling protocol (in section 3), the current modelling systems (in section 4), the data access and quality control (section 5), and a generic inter-comparison of the model simulations (section 6) .

3 Modelling protocol

In order to generate a consistent multi-model dataset, all the WRR1 model simulations followed the same modelling protocol, in particular the meteorological forcing and models output format. The following sub-sections describe in detail the meteorological forcing, the simulations setup and output format.

3.1 Meteorological forcing

For the meteorological forcing, it was decided to use a recent state-of-the-art dataset: the WATCH¹ (Water and Global Change FP7 project) Forcing Dataset ERA-Interim (hereafter WFDEI, Weedon et al. 2014). WFDEI is a follow up dataset of the EU WATCH project (Harding et al. 2011). WFDEI is based on the ECMWF ERA-Interim reanalysis (Dee et al. 2011) with a spatial resolution of $0.5^\circ \times 0.5^\circ$, and temporal frequency of 3 hours for the period 1979-2012 with several bias corrections using gridded observations. Table 3.1 provides an overview of the WFDEI variables. WFDEI provides two sets of precipitation based on different observational datasets corrections, and it was decided to use the CRU (Climatic Research Unit) based dataset that is available for the period 1979-2012.

Table 3.1: Overview of the meteorological forcing, and the correction applied to the original ERA-Interim during the WFDEI processing.

Variable	Definition	Units	Corrections
Wind ⁽¹⁾	3D ⁽⁴⁾ variable: Wind speed at reference level near the surface: 10 meters	m s ⁻¹	None
Tair ⁽¹⁾	3D ⁽⁴⁾ variable: Temperature at a reference level near the surface: 2 meters	K	Elevation using lapse rate; CRU average and average diurnal temperature range
Qair ⁽¹⁾	3D ⁽⁴⁾ variable: Specific humidity at reference level near the surface: 2 meters	kg kg ⁻¹	Via changes in Tair and PSurf
PSurf ⁽¹⁾	2D ⁽⁴⁾ variable: Pressure at the surface	Pa	Via changes in Tair
SWdown ⁽²⁾	2D ⁽⁴⁾ variable: Surface incident shortwave radiation	W m ⁻²	CRU average cloud cover and effects of interannual changes in atmospheric aerosol loading
LWdown ⁽²⁾	2D ⁽⁴⁾ variable: Surface incident longwave radiation	W m ⁻²	Via fixes relative humidity and changes in Tair, PSurf and Qair
Rainf ⁽²⁾⁽³⁾	2D ⁽⁴⁾ variable: Average rainfall (only liquid phase)	Kg m ⁻² s ⁻¹	CRU number of wet days and precipitation totals
Snowf ⁽²⁾⁽³⁾	2D ⁽⁴⁾ variable: Average snowfall (only solid phase)	Kg m ⁻² s ⁻¹	CRU number of wet days and precipitation total

⁽¹⁾ Instantaneous variable at specific time.

⁽²⁾ Mean flux over the previous 3 hours.

⁽³⁾ Total precipitation is given by Rainf+Snowf.

⁽⁴⁾ 2D, 3D refers to the spatial grid, with two dimensions (latitude,longitude) or three dimensions (height,latitude,longitude). The length of the height dimension is equal to one in the current forcing fields. In both bases, there is an extra dimension for the time.

The data was originally downloaded from the WFDEI ftp repository (<ftp.iiasa.ac.at>) and the following changes were applied:

¹ www.eu-watch.org

1. The WFDEI comes with missing data over the ocean. These points were filled (to avoid land-sea mask problems with different models). The original ERA-Interim (ERA-I) forcing data interpolated to the WFDEI grid (bilinear interpolation) was used to fill the missing data of WFDEI. For precipitation, we use the ERA-Interim/Land dataset (Balsamo et al. 2015).
2. Netcdf conventions.
3. Some attributes of the variables were modified to be CF compliant (Climate and Forecast metadata conventions).
4. Among the changes in the variables attributes, Tair, Qair, and Wind were changed from 2 dimensional fields to 3 dimensions fields (time,height,lat,lon) following the ALMA (Assistance for Land-surface Modelling activities) conventions².
5. 1 extra timestep was added in the end of the forcing files (coping from the next month file) so that each file contains the full data needed to run the models for a particular month.
6. Format: netcdf4 - This is done during the conversion of the original files and allows to save disk space by compression.

The forcing dataset is freely available at both 3 hourly and daily frequencies in the data server at:

https://wci.earth2observe.eu/thredds/catalog/ecmwf/met_forcing_v0/catalog.html

The files are organized in folders for each month containing separate files for each variable and can be accessed via direct HTTP download or OPENDAP:

Using HTTP:

[http://wci.earth2observe.eu/thredds/fileServer/ecmwf/met_forcing_v0/\[YEAR\]/\[VAR\]_E2OBS_\[YEAR\]_\[MONTH\].nc](http://wci.earth2observe.eu/thredds/fileServer/ecmwf/met_forcing_v0/[YEAR]/[VAR]_E2OBS_[YEAR]_[MONTH].nc)
 e.g.
http://wci.earth2observe.eu/thredds/fileServer/ecmwf/met_forcing_v0/1992/LWdown_E2OBS_199202.nc
 (copy&paste the link in a browser)

Using OPENDAP:

[http://wci.earth2observe.eu/thredds/dodsC/ecmwf/met_forcing_v0/\[YEAR\]/\[VAR\]_E2OBS_\[YEAR\]_\[MONTH\].nc](http://wci.earth2observe.eu/thredds/dodsC/ecmwf/met_forcing_v0/[YEAR]/[VAR]_E2OBS_[YEAR]_[MONTH].nc)
 e.g.
http://wci.earth2observe.eu/thredds/dodsC/ecmwf/met_forcing_v0/1992/LWdown_E2OBS_199202.nc

Where:

[YEAR]: 1979, ..., 2012
 [MONTH]: 01, ..., 12
 [VAR]: Wind, Tair, Qair, PSurf, SWdown, LWdown, Rainf, Snowf

At the time of preparing this report, four minor issues were found in the WFDEI forcing, that do not affect the overall quality of the model simulations, but should be considered in case some suspicious simulations are found and could be related to these issues:

7. There are some concerns of the energy forcing terms of WFDEI (SWdown, LWdown) over the Amazon region. The problem was in the SW/LW partition in WFDEI, with an underestimation of SWdown and overestimation of LWdown. When comparing WFDEI with the original ERAI data and the GEWEX Surface Radiation Budget dataset (SRB³) we found that the SWdown underestimation was already present in ERAI. This could be related to an overestimation of cloud cover. The overestimation of LWdown in WFDEI, when compared with SRB is mainly due to the corrections applied to WFDEI, since ERAI is similar to SRB. Further analysis would

² http://www.lmd.jussieu.fr/~polcher/ALMA/convention_input_3.html

³ <http://www.gewex.org/srbdata.htm>

require the use of station data to fully evaluate the different datasets, but such analysis will require time, and it is not foreseen before the release of WRR1, but should be considered for WRR2. For example, Iizumi et al. (2014) presented a comparison of different meteorological forcing datasets with station data, and WFDEI shows good quality.

8. In some timestamps there is some noise at night time (about 0.05 W m^{-2}). This was inherited from the original ERA-Interim data. This affects the 00h and 15h steps of December/January/February in all years and days. This results from the processing of the fluxes archived by the atmospheric model in ERA-Interim.
9. Large positive values of $\text{SWdown} > 5 \text{ W m}^{-2}$ at night time in some Islands and coastal points. This was not present in ERA-Interim and was introduced during the WFDEI data processing.
10. Some grid-points were detected with a significant change in the snowfall amounts, and in particular the ratio of snowfall/precip between WFDEI forcing and ERA-Interim. A total of 9 Grid-points were found with a substantial conversion of liquid rainfall (in ERA-Interim) into snowfall (in WFDEI). This conversion was introduced by the WFDEI data processing. For some models, this can lead to a continuous accumulation of snow over those points.

3.2 Simulations setup

The simulations were performed from the 1st of January 1979 to the 31st of December 2012 in a continuous simulation without any kind of data assimilation. The initialization method of the model on the 1st of January 1979 is left to each modelling group to decide. Details on the initialization of each model are given in the sub-sections of section 4. Regarding static fields (e.g. land cover type) each modelling group used their own dataset, as this is considered to be part of the modelling system, and exchanging these fields between models is not straightforward.

3.3 Models output

All models used the same grid for the model post-processing (equal to the meteorological forcing) and the grid-points not represented by the model (e.g. ocean or lakes) are set to missing value in the output. The simulations are available on the server with a daily frequency. For the models that run a sub-daily time-step, the daily means are computed from all model time-steps. The monthly means were computed directly at the server using the climate data operators: `cdo`⁴:

```
cdo -f nc4 -z zip_6 -k grid monmean input.nc output.nc
```

The file format is netcdf4 with compression. The preferred chunking type is for grid access, i.e. chunk sizes of: 1,nlat,nlon (time,lat,lon). This makes the access to a particular full field at any time step fast, however the extraction of grid-point time series can take some time, in particular for the daily data.

The output file names contain a single variable extending the full simulations period following the convention:

e2o_**ID**_**VER**_**DOMAIN**_**FREQ**_**VAR**_**YEARSTART-YEAREND**.nc

11. **ID**: institution identifier (see Table 3.2)
12. **VER**: experiment name. **wrr1** for the water resources reanalysis version 1, other values with different model configurations (see section 5)
13. **DOMAIN**: domain identification. For gridded data, the domain will contain the region information and the last two characters the resolution in minutes (e.g. glob30 for the global simulation at 0.5×0.5). For point data, the domain will contain a single identifier for the point (e.g. GRDC station id).

⁴ <https://code.zmaw.de/projects/cdo>

14. **FREQ**: output frequency: **day, mon, 1hr, fix** (for fixed fields, e.g. land sea mask)
15. **VAR**: variable name contained in the file (see Table 3.3)
16. **YEARSTART-YEAREND**: start and end year denoting the temporal extension (e.g. 1979-2012)

Table 3.2: Institution identifiers in the model outputs

Institution Id	Institution (model)
ecmwf	ECMWF (HTESSEL, see 4.1)
univu	University of Utrecht (PCR-GLOBWB, see 4.5)
metfr	Meteo-France (Surfex-trip, see 4.6)
nerc	NERC (Jules, see 4.2)
jrc	JRC (LISFLOOD, see 4.3)
cnrs	CNRS (Orchidee, see 4.4)
univk	University of Kassel (WaterGap3, see 4.10)
ambio	Ambiotek (WaterWorld, see 4.7)
csiro	ANU/CSIRO (W3RA, see 4.9)
eth	ETH (SWBM, see 4.8)

A list of the requested output variables is presented in Table 3.3. If a model does not represent a certain process, the associated variables are not available on the data sever. Please note that the water/energy fluxes follow the mathematical convention, i.e. positive into the surface and negative from the surface (see details in Table 3.3). For example runoff has a negative signal.

Table 3.3: List of output variables and conventions

Name	long_name (attribute)	standard_name (attribute)	units (attribute)	Definition	Positive direction
Precip	total precipitation	precipitation_flux	kg m ⁻² s ⁻¹	Average of total precipitation (Rainf+Snowf)	downwards
Evap	total evapotranspiration	water_evaporation_flux	kg m ⁻² s ⁻¹	Sum of all evaporation sources, averaged over a grid cell	downwards
Runoff	Total runoff	runoff_flux	kg m ⁻² s ⁻¹	Average total liquid water draining from land	into grid cell
Rainf	rainfall	rainfall_flux	kg m ⁻² s ⁻¹	Average of the total rainfall (liquid phase)	downwards
Qs	surface runoff	surface_runoff_flux	kg m ⁻² s ⁻¹	Runoff from the land surface and/or subsurface stormflow	into gridcell
Qsb	Subsurface runoff	subsurface_runoff_flux	kg m ⁻² s ⁻¹	Gravity drainage and/or slow response lateral flow. Ground water recharge will have the opposite sign.	into gridcell
Qrec	Recharge	N.A	kg m ⁻² s ⁻¹	Recharge from river to the flood plain and from groundwater to soil column	into of gridcell
Qsm	snowmelt	surface_snow_melt_flux	kg m ⁻² s ⁻¹	Average liquid water generated from solid to liquid phase change in the snow	solid to liquid
PotEvap	potential evapotranspiration	water_potential_evaporation_flux	kg m ⁻² s ⁻¹	The flux as computed for evapotranspiration but will all resistances set to zero, except the aerodynamic resistance.	downwards

Name	long_name (attribute)	standard_name (attribute)	units (attribute)	Definition	Positive direction
ECanop	interception evaporation	water_evaporation_flux_from_canopy	kg m ⁻² s ⁻¹	Evaporation from canopy interception, averaged over all vegetation types within a grid cell.	downwards
TVeg	vegetation transpiration	transpiration_flux	kg m ⁻² s ⁻¹	Vegetation transpiration, averaged over all vegetation types within a grid cell.	downwards
ESoil	bare soil evaporation	water_evaporation_flux_from_soil	kg m ⁻² s ⁻¹	Evaporation from bare soil.	downwards
EWater	Open water evaporation	N.A	kg m ⁻² s ⁻¹	Evaporation from surface water storage (lakes, river Chanel, floodplains, etc.)	downwards
RivOut	river discharge	N.A	m ³ s ⁻¹	Water volume leaving the cell	downstream
Dis	point river discharge	N.A	m ³ s ⁻¹	Water volume leaving the cell	downstream
SWnet	Net shortwave radiation	surface_net_downward_shortwave_flux	W m ⁻²	Incoming solar radiation less the simulated outgoing shortwave radiation, averaged over a grid cell	downward
LWnet	Net longwave radiation	surface_net_downward_longwave_flux	W m ⁻²	Incident longwave radiation less the simulated outgoing longwave radiation, averaged over a grid cell	downward
Qle	Latent heat flux	surface_downward_latent_heat_flux	W m ⁻²	Energy of evaporation, averaged over a grid cell	downward
Qh	Sensible heat flux	surface_downward_sensible_heat_flux	W m ⁻²	Sensible energy, averaged over a grid cell	downward
AvgSurfT	Average surface temperature	surface_temperature	K	Average of all vegetation, bare soil and snow skin temperatures	-
Albedo	Surface Albedo	surface_albedo	-	Grid cell average albedo for all wavelengths.	-
LAI	Surface Albedo	leaf_area_index	-	Gridl cell average lead area index	-
SWE	Snow water equivalent	liquid_water_content_of_surface_snow	Kg m ⁻²	Total water mass of the snowpack (liquid or frozen), averaged over a grid cell (including SWEVeg)	-
CanopInt	Total canopy water storage	N.A	Kg m ⁻²	Total canopy interception, averaged over all vegetation types within a grid cell (included both solid and liquid)	-
SWEVeg	SWE intercepted by the vegetation	N.A	Kg m ⁻²	Total water mass of the snowpack (liquid or frozen), averaged over a grid cell and interecepted by the canopy	-
SurfStor	Surface Water Storage	N.A	Kg m ⁻²	Total liquid water storage, other than soil, snow or interception storage (i.e. lakes, river channel or depression storage).	-
WaterTableD	Water table Depth	N.A	M	Depth of the water table (distance from surface)	-

Name	long_name (attribute)	standard_name (attribute)	units (attribute)	Definition	Positive direction
SnowFrac	Snow covered fraction	surface_snow_area_fraction	-	Grid cell snow covered fraction	-
SnowDepth	Depth of snow layer	surface_snow_thickness	M	total snow depth	-
SurfMoist	Surface soil moisture	N.A	Kg m ⁻²	best of 5 cm depth or first model layer	-
RootMoist	Root zone soil moisture	N.A	Kg m ⁻²	Total soil moisture available for evapotranspiration (or up to 1 meter depth if not defined)	-
TotMoist	Total soil moisture	N.A	Kg m ⁻²	Vertically integrated total soil moisture	-
GroundMoist	ground water	N.A	Kg m ⁻²	ground water not directly available for evapotranspiration	-
lsm	Land sea mask	land_area_fraction	-	fraction of land in each cell	
SurfSoilSat	Surface soil saturation	N.A	Kg m ⁻²	saturation soil moisture for the layer reported in SurfMoist	
RootSoilSat	Root soil saturation	N.A.	Kg m ⁻²	saturation soil moisture for the layer reported in RootMoist	
TotSoilSat	Total soil saturation	N.A	Kg m ⁻²	saturation soil moisture for the layer reported in TotMoist	

4 Modelling systems

A generic overview of the modelling systems, acronyms and references is provided in Table 4.1 followed by an overview of each modelling system in the following sub-sections.

Table 4.1: Modelling systems details

Modelling systems	Interception	Evaporation	Snow	Soil	GroundWater	Runoff	Reservoir Lakes	Routing	Water use	Model timestep	References
HTESSEL-CaMa	Yes, single reservoir, potential evaporation	Penman-Monteith	Energy balance, 1 layer	4 Layers	Not represented	Saturation excess	Not represented	CaMa-Flood River channel, floodplains, local Inertial equation	Not represented	1 hour	Balsamo et al. (2011); Yamazaki et al. (2011)
JULES	Yes, single reservoir, potential evaporation	Penman-Monteith	1 composite soil/snow layer	4 layers	Not represented	Infiltration capacity and saturation excess	No	No represented	Not represented	1 hour	(Best et al. 2011); (Clark et al. 2011)
LISFLOOD	Yes, single reservoir, potential evaporation	Penman-Monteith	Degree-day, one layer	2 layers	2 layers	Saturation and infiltration excess	Yes	Double kinematic wave	Yes	1 day	(Burek et al. 2013; Van Der Knijff et al. 2008)
ORCHIDEE	Single reservoir structural resistance to evaporation	Bulck ETP (Barella-Ortiz et al. 2013)	1 moisture layer, 1-5 thermodynamic layers	11 Layers	2 reservoirs	Green-Ampt infiltration + gravitational drainage	No	linear cascade of reservoirs at the sub-grid level	irrigation only	900s energy balance, 3hours routing	(d'Orgeval et al. 2008)
PCR-GLOBWB	Single layer, subject to open water evaporation	Hamon (tier 1) or imposed as forcing	Temperature based melt factor	2 Layers	represented by third soil layer, subject to drainage via linear reservoir	Saturation excess	reservoirs parameterized from GRanD, lakes from GLWD; (tier 1 only including lakes)	kinematic wave with floodplains or travel time approach (tier 1)	Not represented in tier 1	1 day	(Sutanudjaja et al. 2014); (van Beek et al. 2011)

Modelling systems	Interception	Evaporation	Snow	Soil	GroundWater	Runoff	Reservoir Lakes	Routing	Water use	Model timestep	References
SURFEX-TRIP	Yes, single reservoir, potential evaporation	Penman-Monteith	Energy and mass balance, 12 layers	14 Layers	Only a deep-water reservoir that only delays the deep flow contribution to the surface river	Horton and Dunne runoff (infiltration capacity and saturation excess)	Not represented	TRIP with stream and deep-water reservoir at 0.5°	Not represented	900s for ISBA 3600s for TRIP	(Decharme et al. 2013) (Decharme et al. 2011)
WaterWorld	No	Yes, modified penman	Energy balance model	1 Layer	Saturation and hortonian	Yes	Yes	Yes	Yes for agriculture, and according to population	Monthly	(Mulligan and Burke 2005), (Mulligan 2013)
SWBM	No	Inferred from net radiation	Degree-day approach, 1 Layer	1 Layer	Not represented	Inferred from precipitation and soil moisture	Not represented	Not represented	Not represented	1 Day	(Orth and Seneviratne 2015)
W3RA	Yes, potential	Penman-Monteith	Yes, mass balance	1 Layer	Yes	Yes	yes	kinematic wave	Not represented	1 day	(van Dijk et al. 2013)
WaterGAP3	Yes, single reservoir	Priestley-Taylor	Degree-day, 1 layer	1 layer	Renewable groundwater, single-layer linear reservoir	Beta function	Yes	Manning-Strickler	Yes, represented for five sectors: irrigation, livestock farming, domestic, manufacturing, thermal elec. production	1 day	Verzano (2009) Flörke et al. (2013)

4.1 HTESSEL-CaMa

The land surface model (LSM) HTESSEL (Hydrology Tiled ECMWF Scheme for Surface Exchanges over Land) computes the land surface response to atmospheric conditions, and estimates the surface water and energy fluxes and the temporal evolution of soil temperature, soil moisture content, vegetation interception and snowpack conditions. These are computed for each grid-point independently, i.e. there is no horizontal interaction between each surface/soil column. At the interface to the atmosphere each grid box is divided into fractions (tiles), with up to six fractions over land (bare ground, low and high vegetation, intercepted water and shaded and exposed snow)(see Figure 4.1). Vegetation types and cover fractions are derived from an external climate database, based on the Global Land Cover Characteristic (Loveland et al. 2000). The grid box surface fluxes are calculated separately for each tile, leading to a separate solution of the surface energy balance equation and skin temperature.

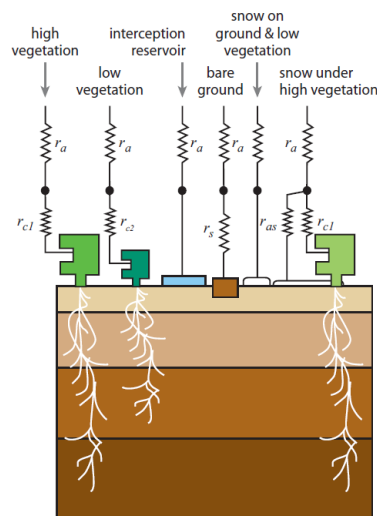


Figure 4.1: HTESSEL surface and subsurface discretization scheme

The interception reservoir is a thin layer on top of soil/vegetation, collecting liquid water by the interception of rain and the collection of dew, and evaporating at the potential rate. The maximum capacity of this reservoir is a function of the grid-box leaf area index.

The snow represents an additional layer on top of the upper soil layer, with independent prognostic, thermal and mass contents (Dutra et al. 2010). The snowpack is represented by a single layer with an evolution of snow temperature, snow mass, snow density, snow albedo, and a diagnostic formulation for the snow liquid water content.

Below the surface, the soil is discretized in four layers (0.07, 0.21, 0.72 and 1.89 m) for the water and energy transfer. Soil heat transfer follows a Fourier law of diffusion, modified to take into account soil water freezing/melting (Viterbo et al. 1999). The vertical movement of water in the unsaturated zone of the soil matrix follows Richards's equation and Darcy's law. Hydraulic conductivity and diffusivity are derived using van Genuchten formulation and 6 soil textures globally distributed are used. Water movement is limited in the case of partially frozen soil, by reducing the hydraulic conductivity and diffusivity. The top boundary condition is precipitation minus evaporation minus runoff, and the bottom boundary condition assumes free drainage.

A resistance parameterization is used to calculate the turbulent fluxes (see Figure 4.1), and in particular for evaporation the aerodynamic resistance is added to the canopy resistance. The canopy resistance is a function of downward short-wave radiation, leaf area index, soil moisture, water vapor deficit and a minimum stomatal resistance. For the soil moisture dependence, the fraction of roots in each soil layer is also considered.

Water leaves the soil column in the bottom layer as free drainage, and this is denoted as sub-surface runoff. At the surface, a variable infiltration rate that accounts for the sub-grid variability related to orography is used to compute the surface runoff (Balsamo et al. 2009).

The surface and sub-surface runoff generated by HTESSEL are feed to the Catchment-based Macro-scale Floodplain model (CaMa-Flood, Yamazaki et al. (2011). CaMa-Flood simulates the hydrodynamics in continental-scale rivers. The entire river network of the world are discretized to hydrological units named unit-catchments for achieving efficient flow computation at the global scale (Yamazaki et al. 2009). The water level and flooded area are diagnosed from the water storage at each unit-catchment using the sub-grid topographic parameters of the river channel and floodplains. The river discharge and flow velocity are calculated with the local inertial equation along the river network map which prescribes the upstream-downstream relationship of unit-catchments. The time evolution of the water storage, the only prognostic variable, is solved by the water balance equation which considers inflow from the upstream cells, outflow to the downstream cell and input from runoff forcing at each unit-catchment.

The HTESSEL-CaMA simulations were carried out at the default 0.5x0.5 resolution. The land use maps (e.g. type of vegetation and cover), mean climatologies of leaf area index and snow-free surface albedo were prescribed from the data used currently in operational weather forecasts at ECMWF. The simulations were performed only over land points and a 10 year spin-up was carried out: initial run from 1st Jan 1979 to 1st Jan 1989, and land surface state in Jan 1989 was used to initialize the main simulation starting on the 1st January 1979. In both HTESSEL and CaMa-Flood the default set of parameters were used, with no particular calibration performed for these simulations.

4.2 JULES

JULES (the Joint UK Land Environment Simulator) is a community land surface model that has evolved from the Met Office Surface Exchange Scheme (MOSES). JULES represents different land surface processes (surface energy balance, hydrological cycle, carbon cycle, leaf phenology, etc.) and allows them to interact with each other (Figure 4.2).

JULES has a tiled model of sub-grid heterogeneity with separate surface temperatures, short-wave and long-wave radiative fluxes, sensible and latent heat fluxes, ground heat fluxes, canopy moisture contents, snow masses and snow melt rates computed for each surface type in a grid-box. Nine surface types are used: five Plant Functional Types (PFTs); broadleaf trees, needleleaf trees, C3 (temperate) grass, C4 (tropical) grass and shrubs, and four non-vegetation types: urban, inland water, bare soil and land-ice. Fractions of surface types within each land-surface grid-box are read from an ancillary file, derived from an external database (Global Land Cover Characteristics Data Base Version 2.0). Air temperature, humidity and wind-speed above the surface and soil temperatures and moisture contents below the surface are treated as homogeneous across a grid-box.

The surface energy balance for each tile includes fluxes of sensible heat and moisture, and latent heat of vaporization for snow-free tiles or sublimation for snow-covered or ice tiles. The heat flux into the ground, combining radiative fluxes below vegetation canopies and conductive fluxes for the unvegetated fraction, is parameterized as a function of the thickness and temperature of the surface soil layer. Radiative canopy fraction is calculated separately by a Canopy Heat Capacity model.

Surface evaporation is drawn from soil, canopy and snow moisture stores. Evaporation from saturated parts of the surface (lakes, wet vegetation canopies and snow) is calculated at the potential rate (i.e. subject to an aerodynamic resistance only). Evaporation from transpiring vegetation is controlled by the canopy conductance. The ability of vegetation to access moisture at each level in the soil is determined by root density. The evaporative flux extracted from each soil layer is dependent on the soil moisture availability factor. Bare-soil evaporation is extracted from the surface soil layer. A fraction of the tile is assumed to be saturated and hence has aerodynamic resistance only.

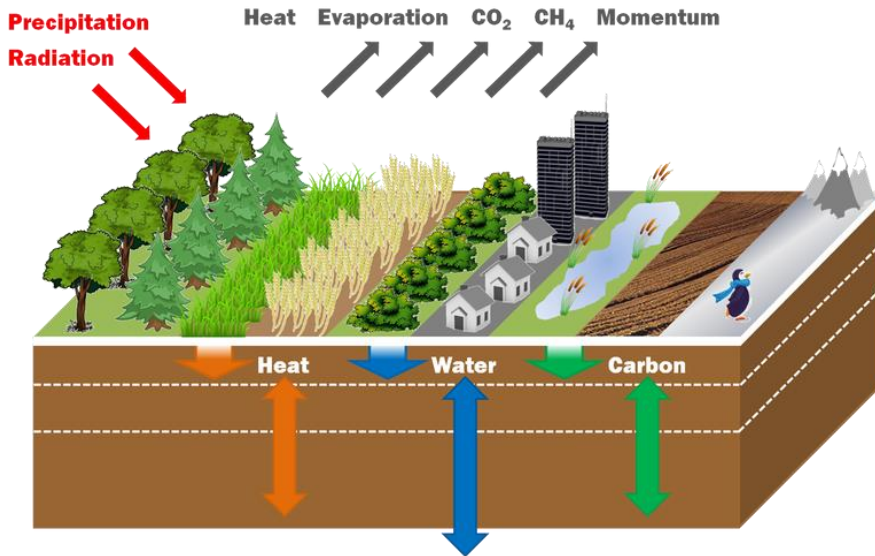


Figure 4.2: Jules model concept.

The initial partitioning of precipitation into interception, throughfall, runoff and infiltration is applied separately on each tile. Essentially, the rainfall rate is assumed to be distributed exponentially across the area. In addition, if the rainfall is convective, then it is assumed to cover only 30% of the area. An additional saturation excess runoff production is calculated using a Probabilistic Distributed Model (PDM; Moore, 1985) approach.

Below the surface, the soil is discretized in four layers (0.10, 0.25, 0.65 and 2.0 m) for the water and energy transfer. Subsurface temperatures are updated using a discretized form of the heat diffusion equation, which is coupled to the soil hydrology module. It includes soil water phase changes and the associated latent heat, the soil thermal characteristics are dependent on soil moisture content (liquid water and ice). The temperature of the n th soil layer is incremented by the diffusive heat fluxes into and out of the layer, and the net heat flux advected from the layer by the moisture flux.

The soil hydrology component of JULES is based on a finite difference approximation to the Richards' equation (Richards, 1931). The total soil moisture content within a soil layer is incremented by the diffusive water flux flowing in from the layer above, the diffusive flux owing out to the layer below, and the evaporation extracted directly from the layer by plant roots and soil evaporation which is calculated from the total evaporation, based on the profiles of soil moisture and root density. The water fluxes are given by the Darcy equation which depends on the hydraulic conductivity and the soil water suction. To close the model it is necessary to assume forms for the hydraulic conductivity and the soil water suction as a function of the soil moisture concentration (Brooks and Corey, 1964).

Soil carbon storage is increased by the total litterfall and reduced by microbial soil respiration which occurs at a rate dependent on soil moisture, temperature and soil carbon content.

Leaf photosynthesis is dependent on a number of environmental variables as well as the internal CO₂ concentration. Stomatal openings are the pathways through which both water and carbon dioxide are exchanged between vegetation and the atmosphere. Consequently, net leaf photosynthesis and stomatal conductance to water vapour are linked. The fluxes of carbon and water vapour are proportional to the gradient of water vapour and carbon dioxide respectively.

The JULES simulation was carried out at the default 0.5x0.5 resolution. The simulation was performed only over land points and a 10 year spin-up was carried out: initial run from 1979 to 1989, and land surface state in Jan 1989 was used to initialize the main simulation starting on the 1st January 1979. The JULES default set of parameters for global simulations were used, with no particular calibration performed for these simulations.

4.3 LISFLOOD

LISFLOOD is a spatially distributed, grid-based rainfall-runoff and channel routing model that has been primarily for the simulation of large river basins. Figure 4.3 gives an overview of the structure of LISFLOOD. As the figure shows, the model is made up of a two-layer soil water balance sub-model, sub-models for the simulation of groundwater and subsurface flow (using two parallel interconnected linear reservoirs), a sub-model for the routing of surface runoff to the nearest river channel, and a sub-model for the routing of channel flow (not shown in the figure). The processes that are simulated by the model include snow melt (not shown in Figure 4.3), infiltration, interception of rainfall, leaf drainage, evaporation and water uptake by vegetation, surface runoff, preferential flow (bypass of soil layer), exchange of soil moisture between the two soil layers and drainage to the groundwater, subsurface and groundwater flow, and flow through river channels. Upward vertical soil moisture and groundwater flow (capillary rise) are not simulated, and neither are deep groundwater systems. This poses some limitations on the use of LISFLOOD in areas that are either very dry or have a hydrology that is heavily influenced by deep groundwater, or combinations of both. For LISFLOOD we have aimed to select process descriptions that make the best use of available prior data – thus reducing the number of calibration parameters, but we have tried to avoid process descriptions that are overly complex, computationally demanding or irrelevant at the scale of large catchments. LISFLOOD is driven by the following meteorological variables: precipitation intensity, P (mm/day), potential (reference) evapotranspiration rate of a closed canopy, ET_0 (mm/day), potential (reference) evaporation rate from a bare soil surface, ES_0 (mm/day), potential evaporation rate from an open water surface, EW_0 (mm/day), and average 24-hour temperature, T_{avg} (uC). ET_0 , ES_0 and EW_0 are all calculated outside the model using the Penman-Monteith equation as given by (Supit et al. 1994). See (Van Der Knijff et al. 2008) and (Burek et al. 2013) for detailed descriptions of the individual processes.

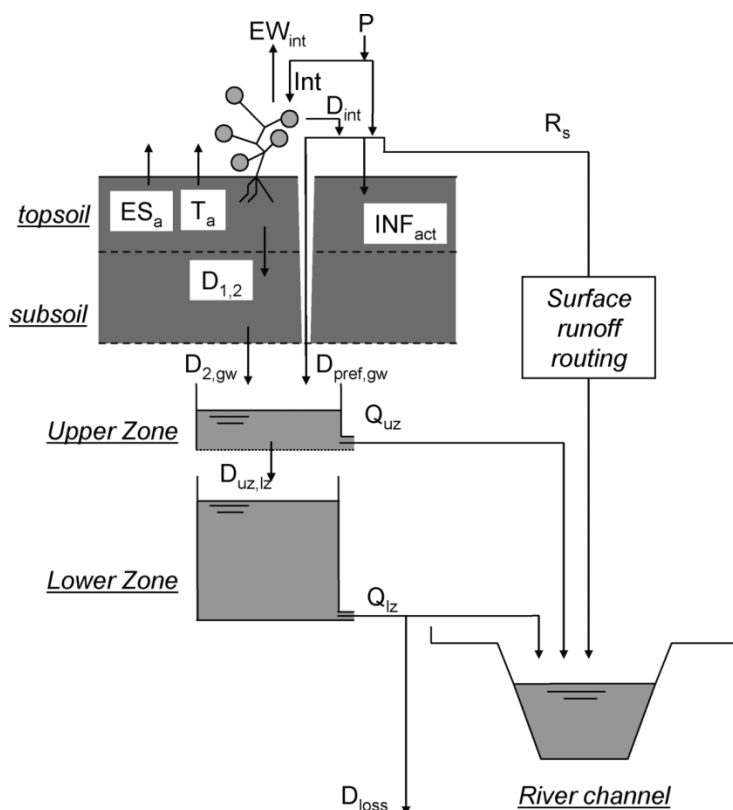


Figure 4.3: Overview of the LISFLOOD model. P = precipitation; Int = interception; EW_{int} = evaporation of intercepted water; D_{int} = leaf drainage; ES_a = evaporation from soil surface; T_a = transpiration (water uptake by plant roots); INF_{act} = infiltration; R_s = surface runoff; $D_{1,2}$ =

drainage from top- to subsoil; D2,gw = drainage from subsoil to upper groundwater zone; Dpref,gw = preferential flow to upper groundwater zone; Duz,lz = drainage from upper to lower groundwater zone; Quz = outflow from upper groundwater zone; Ql = outflow from lower groundwater zone; Dloss = loss from lower groundwater zone. Note that snowmelt is not included in the figure (even though it is simulated by the model; from (Van Der Knijff et al. 2008).

For Tier 1 simulations, the model was run at a daily temporal and 0.1° spatial resolution, although the channel routing processes were run at an hourly time step. Potential evaporation was computed from the provided forcing WFDEI dataset, with surface albedo derived from a monthly climatology based on the European Space Agency (ESA) GlobAlbedo product (Muller et al. 2011). Soil properties were taken from SoilGrids1km (Hengl et al. 2014). Digital elevation data are obtained from the SRTM for latitudes <60°N and GTOPO30 for latitudes >60°N. Land cover was derived from GLobCover2009 (Bontemps et al. 2011) and LAI from SPOT-VGT. In its current state the model has 11 calibratable parameters, which were calibrated for 24 large catchments around the globe and set to default values for the remaining part of the land surface.

4.4 ORCHIDEE

The version of ORCHIDEE used in this article works at three different scales: (i) the energy balance is solved on 0.5°× 0.5° grid boxes, which is the scale of the forcing used; (ii) the hydrological balance is solved separately on three different tiles that make up each grid box - the size of the tiles depend on the distribution of vegetation; and (iii) the river flows are computed through basins defined at a 0.5× 0.5 scale.

Here the hydrological module and the routing module are more specifically described. The full documentation of the model is available at <http://forge.ipsl.jussieu.fr/orchidee/wiki/Documentation>.

The hydrological module used to produce the tier-1 simulations is fully described and tested in (D'Orgeval 2006). It is based on developments by (de Rosnay et al. 2000; de Rosnay et al. 2002). Partitioning between surface infiltration and runoff is computed through a time-splitting procedure. This allows to solve the surface infiltration of precipitation with a finer timestep than 30 minutes. The spatial heterogeneity of the local maximum infiltration rates is approximated by an exponential probability density distribution (Decharme et al. 2006; Yu 2000). The vertical diffusion of water in the soil column is solved by the Fokker-Planck equation with van Genuchten (van Genuchten 1980) parameters. Bare soil evaporation is the maximum upward hydrological flux permitted by the diffusion if this flux is inferior to potential evaporation. An adapted (Monsi and Saeki 1953) law is used for bare soil evaporation under vegetation. Water extraction from roots is determined by an exponential root profile (de Rosnay and Polcher 1998) and free drainage is the boundary condition at 2m below the surface.

13 different vegetation types are defined and the default map is derived from the IGBP map with Olson classification (de Rosnay and Polcher 1998). Vegetation types are grouped into 3 ensembles (bare soil, trees, and grass/crop). Transpiration and interception loss are computed separately for each vegetation type, but the induced throughfall and root uptake are aggregated per vegetation ensemble. Therefore, in each grid box, the hydrological balance is computed for three tiles corresponding to the 3 different vegetation ensembles. 3 different soil types are defined and the default map is derived from a dataset by (Reynolds et al. 2000).

The dominant soil type over a grid box is used for each tile in the grid box. New parametrizations have been introduced to represent three infiltration processes (surface infiltration, deep-soil infiltration, root-zone infiltration) that are considered to be important to accurately represent the West African water cycle. Parameters for this version of ORCHIDEE have been fixed in accordance with validations

against Hapex-Sahel observations (Goutorbe et al. 0001). More details are provided in the description of the parametrizations below and in (D'Orgeval 2006).

Depending on the slope of the land surface, the surface runoff may infiltrate, especially through small pond systems that are common in West Africa (Cappelaere et al. 2003; Peugeot et al. 2003). In ORCHIDEE, infiltration is allowed in case of slopes below 0.5%. The compactness of the soil increases with depth (z) as the smallest particles tend to percolate towards the bottom of the soil (Beven 1984 ; Beven and Germann 1982). In ORCHIDEE, the saturated conductivity is modified in a similar way to what is done in (Decharme et al. 2006). The main differences are that the conductivity is constant from 0 to $z_l=0.3m$, and can be decreased by a factor 5 at most. This factor is chosen to roughly correspond to a change of soil type from coarse to medium or medium to fine.

The routing module is based on (Hagemann and Dümenil 1997) and (Miller et al. 1994). Surface, subsurface runoff, and river fluxes are routed through three different reservoirs in each basin of each grid box (see reservoirs V_i , $i= 1,2,3$ for basins B , B' , ... in Figure 4.4). Each reservoir has a different time constant which only depends on the mean slope of the river and on three constants fixed globally (one per reservoir type). A floodplain module is included in this version of ORCHIDEE to deal with swamps and floodplains such as the ones observed in the Niger Inner Delta or in the Congo basin.

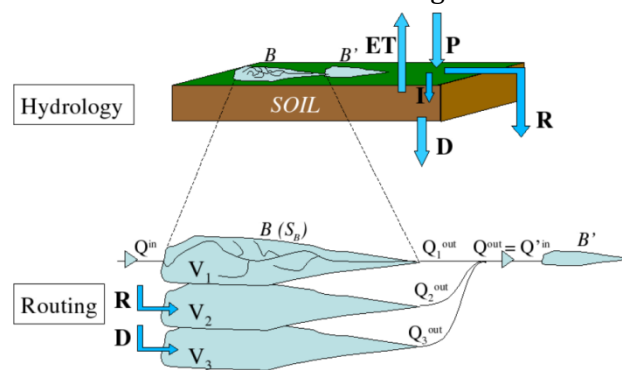


Figure 4.4: ORCHIDEE river routing scheme. The hydrology module computes the partitioning of precipitation (P) into infiltration (I) and surface runoff (R) and then into evapotranspiration (ET) and subsurface runoff (D) for each grid box

The model was first spun up with a simulation from 1st of January 1979 to 31st of December 1990. This simulation started with an average soil moisture and empty aquifers but after the 10 years discharge of the rivers has reached equilibrium. The simulation distributed then used the state variables of the 1st of January 1991 of this first run and covered to the period 1st of January 1979 to 31st of December 2012.

4.5 PCR-GLOBWB

The global hydrological model PCR-GLOBWB (PCRaster GLOBal Water Balance) is a leaky bucket type of model providing a grid based representation of terrestrial hydrology. PCR-GLOBWB is forced by temperature, precipitation and reference potential evapotranspiration. PCR-GLOBWB responds to the prescribed atmospheric conditions through simulating the resulting fluxes and changes in the water content of its different storages (i.e. canopy interception, snow, soil, groundwater, channels and water bodies) for the land and water surface within each cell. This model concept is illustrated in Figure 4.5.

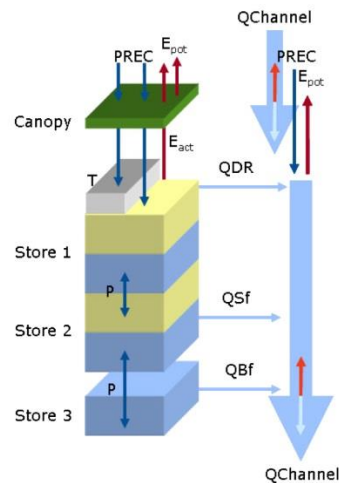


Figure 4.5: PCR-GLOBWB model concept.

Depending on temperature, precipitation can either fall as rain or snow, be partly intercepted by vegetation or reach the surface directly. Intercepted water is subject to open water evaporation. On the basis of the snow module of HBV (Bergström 1995) snow in PCR-GLOBWB accumulates if air temperature is low enough (below 0°C). For temperatures above freezing point, snow melts proportionally by means of a melt factor and is added to the liquid precipitation reaching the surface. At the soil surface, the incoming water is partitioned into direct runoff and infiltration that enters the upper of two vertically stacked soil layers with maximum depths of 0.3m and 1.2m respectively. The amount of direct runoff corresponds predominantly with saturation-excess overland flow and is dependent on the degree of saturation and the distribution of the water holding capacity within each cell (Todini 1996). The sub-grid variability of the water holding capacity is accounted for by the Improved Arno Scheme (Hagemann and Gates 2003). The two soil layers are underlain by a third groundwater layer which represents the deeper part of the soil that is exempt from any direct influence of vegetation and where groundwater accumulates. Vertical water fluxes between the layers are calculated based on Darcy's law and are driven by the layers' effective degree of saturation (Clapp and Hornberger 1978). Capillary rise can occur in case evaporation from the soil layers is large and groundwater is close to the surface. Where percolation at the base of the soil is impeded, the accumulated soil moisture can drain laterally as interflow. Net recharge (percolation minus capillary rise) replenishes the groundwater store. Additionally, river water can infiltrate along the bed if the gradient is directed into the groundwater reservoir. For each cell, drainage from the groundwater storage, sustaining base flow, is described by means of a linear reservoir (Kraaijenhoff van de Leur 1958).

The drainage components runoff (QDR), interflow (QSf) and base flow (Qbf) (see Figure 4.1) eventually accumulate as discharge which is routed along a river network. The routing is based on the kinematic wave with the momentum equation based on Manning's equation or can alternatively be calculated with a more computationally efficient travel time approach (Van Deursen 1995). The subdivision into the fraction land and open water within each cell is based on the area covered by channels, lakes and reservoirs. From all water surfaces water can be lost by evaporation.

Reference potential evaporation in PCR-GLOBWB can either be prescribed as input (forcing) or calculated directly on the basis of temperature and day length (Hamon 1961). Specific evapotranspiration rates are obtained using crop factors and drawn from each of the different water stores or transpired by the vegetation.

For the land surface in PCR-GLOBWB sub-grid variability is included with regards to land cover; for natural conditions, this is subdivided into short and tall vegetation on the basis of the GLCC dataset (USGS EROS Data Center 2002). This may be expanded to include agricultural land cover types. Vegetation phenology and crop calendars are then prescribed by repeating a specific annual course. Sub-grid variations in soil and hydrolithological properties are derived from global data sources (GLiM (Gleeson et al. 2011), FAO Soil Map of the World) and assigned as effective value per land cover type. A

noticeable exception is the distribution of the water holding capacity of the Improved Arno Scheme that is parameterized by its mean and minimum value and a shape factor, representing the combined effect of soil and vegetation properties. The distribution of the surface elevation within each cell, is described using a cumulative function of the 1×1 km Hydro1k data set (USGS EROS Data Center 2006).

In addition to agriculture further anthropogenic interference with the global water cycle can be included optionally by considering dynamic withdrawal, allocation and consumptive use of ground- and surface water resources, corresponding return flows of unconsumed water, and more than 6000 reservoirs of the GRanD database (Lehner et al. 2011).

For Tier 1 of Earth2Observe, the PCR-GLOBWB simulations were carried out at 0.5°×0.5° spatial and daily temporal resolution. To provide a baseline reference run only “natural” (non-humanly modified) components of the water cycle were considered. Water was routed through the river network using the travel time approach and reference potential evapotranspiration was calculated using the Hamon method. A 68 year spin-up was carried out by performing two initial back-to-back runs from 1979 to 2012 prior to the definite run.

4.6 SURFEX-TRIP

The SURFEX modelling system (Masson et al. 2013) of the CNRM uses the ISBA land surface model to compute the soil/snow/vegetation energy and water budgets and the TRIP river routing model to simulate the river flow at the global scale.

ISBA contains the basic physics of the land surface and requires only a limited number of parameters, which depend on the type of soil and vegetation. The present version solves the one dimensional Fourier law for soil temperature and the mixed form of the Richards equation for soil moisture. The closed-form equations between the soil moisture and the soil hydrodynamic parameters, such as the soil matric potential and the hydraulic conductivity, are determined according to the Brooks and Corey model (Decharme et al. 2011). A discretization with 14 layers over 12m depth is used. As shown in Figure 4.6, the hydrological soil depth varies according to the soil/vegetation surface types while the soil temperature is computed throughout the 12m. For example, hydrological depths for grass or crops are near 1.5m or 2m. The soil temperature and moisture nodes are collocated over this superficial hydrological soil column. To extend the temperature profile up to a depth of 12 m, the soil water content is extrapolated to each deeper nodes (Decharme et al. 2013). Note that over potential permafrost area the hydrological depth reaches 12m to well represent soil freezing/melting processes throughout the soil column.

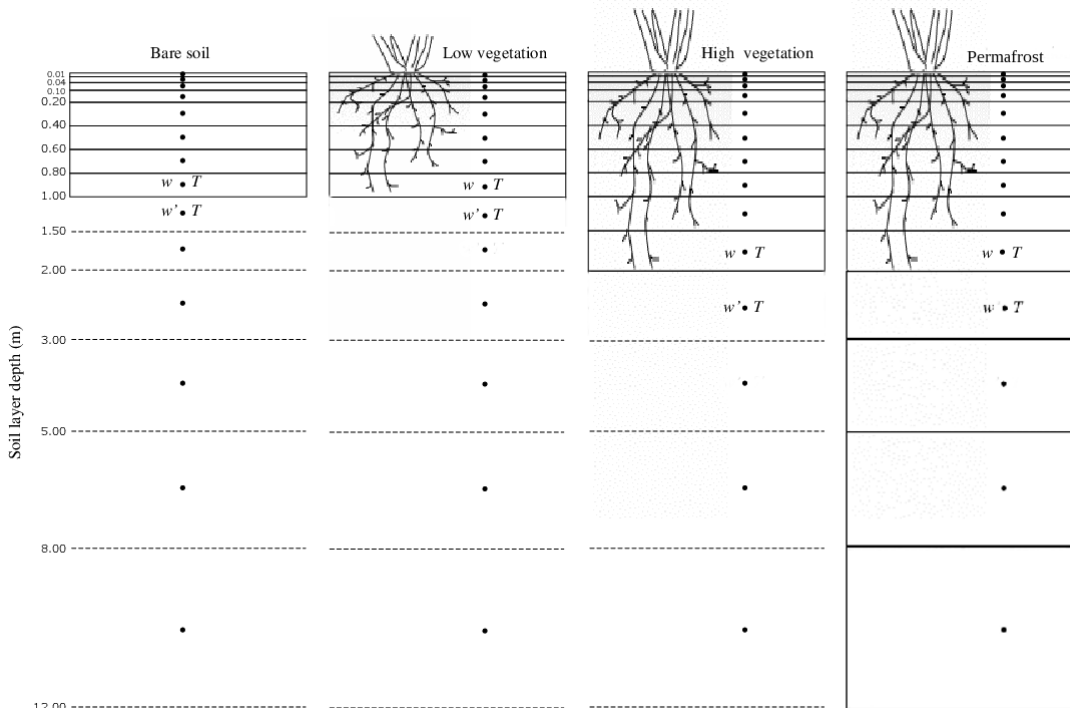


Figure 4.6: Schematic representation of the ISBA soil hydrological and thermal column for four soil/vegetation types. The soil temperature, T , and moisture, w , nodes are collocated. To extend the temperature profile up to a depth of 12 m, the soil water content is extrapolated to each deeper nodes.

Hydrodynamic and thermal soil properties account for the amount of clay, sand and organic carbon present in the soil and given by the HWSD global database (<http://webarchive.iiasa.ac.at/Research/LUC/External-World-soil-database/HTML/>). For the snowpack, a discretization using 12 layers allows the explicit representation of some snow key processes as its viscosity, its compaction due to wind, its age and its albedo on the visible and near infrared spectra.

In terms of hydrology, the soil water balance accounts for infiltration, land surface evapotranspiration, and total runoff. The infiltration rate is given by the difference between the throughfall rate and the surface runoff. The throughfall rate is the sum of the rainfall not intercepted by the canopy, the dripping from the interception reservoir, and the snowmelt from the snowpack.

Water for soil evaporation is drawn from the superficial layer of a thickness of 1 cm. This soil evaporation is weighted by the relative humidity of this superficial layer. This relative humidity evolves non linearly with the superficial water content, allowing that the soil evaporation is maximum for a superficial water content greater than the water content at field capacity specified as matric potential at -0.33 bar. The water used for plant transpiration is removed throughout the root zone in which the roots are asymptotically distributed. Surface resistance in the formulation of transpiration is proportional to the root zone water stress and the stomatal resistance from the Ag-s vegetation interactive scheme (Calvet et al. 1998). This scheme allows to explicitly simulate the Leaf Area Index (LAI). Plant transpiration stops when the root zone water content is below the usual water content at wilting point, corresponding to a matric potential of -15 bar.

The total runoff is composed of the surface runoff, a lateral subsurface flow in the topsoil, and a free drainage condition at the bottom of the hydrological soil column that is simply equal to the hydraulic conductivity of the last hydrological node. The Dunne runoff and lateral subsurface flow within the topsoil is computed via a subgrid distribution of the topography using a simple TOPMODEL approach. The Horton runoff is solved using a subgrid exponential distribution of rainfall intensity and the maximum soil infiltration capacity. This maximum infiltration capacity is computed using a Green-Ampt approach over a depth close to 10cm accounting for frozen soil conditions.

The present TRIP version uses a global river channel network at 0.5° resolution. It is based on a two prognostic equations for the surface stream water and the deep-water mass within each grid cell of the hydrologic network. The streamflow velocity is assumed constant and uniform at 0.5 m.s⁻¹ while the deep-water feeds the surface stream reservoir with a time delay factor of 30 days (Decharme et al. 2010).

The SURFEX simulations were carried out at the default 0.5x0.5 resolution. The type of cover, decadal mean climatologies of snow-free albedo, and soil hydrological depth were prescribed from the ECOCLIMAP database (Faroux et al. 2013). The simulations were performed only over land points and a 20 year spin-up was carried out using two time the 1979-1988 period. In both ISBA and TRIP the default set of parameters were used, with no particular calibration performed for these simulations.

4.7 WaterWorld

WaterWorld is a raster-based model that calculates inputs of wind-driven rainfall (after Arazi et al. (1997)) and fog (Mulligan 2013), and combines these with an energy driven assessment of potential evapotranspiration (PET), then modifies PET by the available leaf area to calculate AET (Mulligan 2013). Rainfall below 0C falls as snow and snow accumulation and melt is calculated using an energy budget model. Wind-driven rainfall plus fog (cloud water interception – CWI) inputs minus AET plus snowmelt determines the water balance. This can be cumulated downstream using a drainage direction network calculated by the system globally from the hole-filled 1 km SRTM (Jarvis et al. 2008) or the 90 m SRTM (Farr and Kobrick 2000) data using the D8 algorithm. WaterWorld includes modules for distribution of rainfall through interaction with wind, occult precipitation through CWI inputs, solar radiation receipt, PET and AET on the basis of climate and vegetation cover, water balance and its cumulation downstream as runoff. There is also a simple model for soil erosion by wash. The model calculates monthly and annual hydrological variables for a baseline representing land cover for the year 2000 and mean 1950–2000 climate.

The WaterWorld V. 1.0 model equations are outlined in detail in (Mulligan and Burke 2005) and in the model documentation with the model at www.policysupport.org/waterworld, and are discussed further in Mulligan (2013) (see appendix at <http://www.iwaponline.com/nh/044/017.pdf>). Version 2 includes snow and ice. Version 3 includes a subsurface component that models infiltration, throughflow and baseflows (see Figure 4.7).

WaterWorld simulations were not included in WRR1 due to the high resolution nature of model, and will be used in specific case studies.

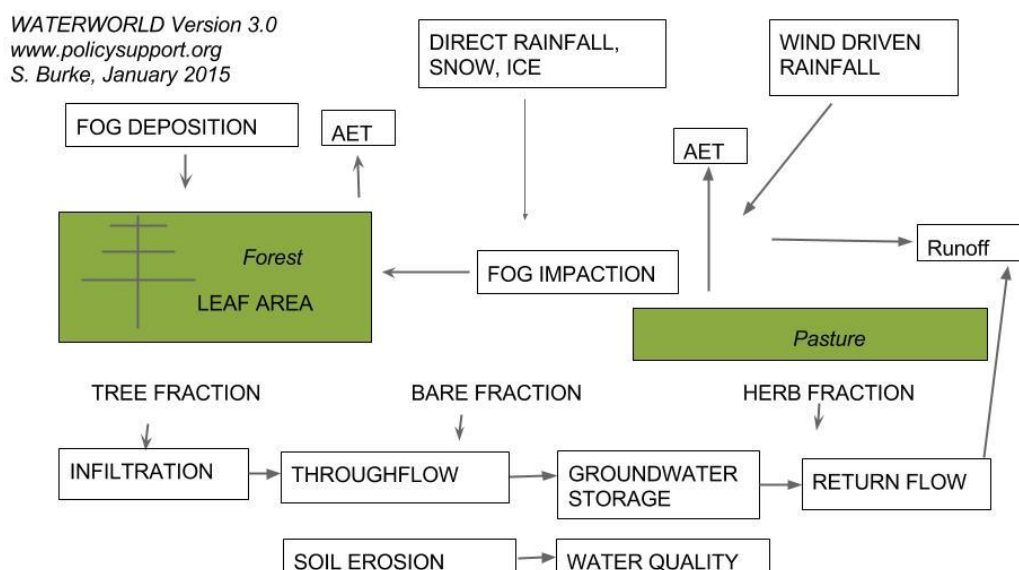


Figure 4.7: Schematic of WaterWorld

4.8 SWBM

The conceptual hydrological model Simple Water Balance Model (SWBM) derives soil moisture, evapotranspiration (ET) and runoff from meteorological information alone. The model was initially proposed by Koster and P. Mahanama (2012), and we employ the version introduced by Orth and Seneviratne (2013) (referred to as OS13 in the following) which is adapted to the daily time scale. The model is based on the water balance equation; soil moisture at the beginning of time step $n + 1$ is computed from observed precipitation accumulated during time step n , along with modelled, accumulated evapotranspiration and runoff. We use in this study a time step of 1 day. ET and runoff are obtained through the assumption that they depend solely on soil moisture when normalized with net radiation and precipitation, respectively. For this purpose, soil moisture is scaled with the water holding capacity of the soil. To represent these two dependencies, the model uses several parameters: (i) two parameters determining the shape of the ET/runoff-soil moisture relationship, (ii) a parameter to limit the maximum possible ET, such that not all net radiation is transformed into ET, and (iii) the water holding capacity of the soil used to scale the soil moisture content. These parameters are reflecting characteristics of soil and vegetation in the model.

The SWBM also considers snow through a degree-day approach with an assumed threshold temperature of 1°C . Snow melts above this temperature, where the melting intensity depends linearly on temperature as determined by a melting parameter. In the OS13 model version, snow is formed from precipitation if the temperature is below the threshold. In this study, snow is also assumed to (partly) form if the temperature is slightly above the threshold; 100%, 50%, 0% of the precipitation form snow at 0°C , 1°C , 2°C , respectively. In case of melting snow we extended the OS13 model version such that the required energy is subtracted from the available net radiation of the particular day.

The OS13 model version incorporates a delayed formation of streamflow to account for the (sub-surface) transport of runoff water to the stream-gauge site, whereby the runoff water is stored in a groundwater storage before it is transformed into streamflow. Even if this mechanism is crucial to estimate daily streamflow dynamics we excluded it from the model because (i) this reduces the computational effort considerably through the removal of a parameter and because delayed streamflow is not calculated and (ii) it does not impact soil moisture and ET. All results related to runoff in this study are only valid on the monthly time scale where runoff and streamflow are rather similar.

To find an optimal parameter set, we sample the entire parameter space. For this purpose, we employ 300 parameter sets, where we choose each parameter randomly from an meaningful range. This range is derived for each parameter from a set of values from observation-based calibration results of the SWBM in Orth and Seneviratne (2014), where the model is calibrated in 400 near-natural catchments across Europe using observed streamflow. To minimize the impact of outliers we use the 5% and 95% quantile of the 400 inferred values of any parameter as bounds for its range. Random values for any parameter are then derived from 20 equally spaced values that span the whole derived range of the considered parameter. Following a thorough validation of all parameter sets against several independent data sets representing multiple hydrological variables across Europe (Orth and Seneviratne 2015), we identify a best-performing model calibration which is applied across the entire globe in this project. An overview of the model parameters is given in Table 4.2

Table 4.2: Overview of model parameters used by SWBM.

Parameter	Meaning	Value
Water holding capacity	Maximum water storage	971 mm

Runoff function shape parameter	Sensitivity of (normalized) runoff to soil moisture	10.4
ET function shape parameter	Sensitivity of evaporative fraction to soil moisture	1.14
Maximum normalized ET	Maximum fraction of net radiation that can be transformed into ET	0.67
Melting parameter	Speed of snow melting	3.9 mm/K

4.9 W3RA

The Water Resources Assessment (W3RA) system is based on the landscape hydrology component model of the AWRA system (AWRA-L version 1.0) (van Dijk 2010a; Van Dijk 2010b. AWRA-L can be considered a hybrid between a simplified grid-based land surface model and a nonspatial (or so-called “lumped”) catchment model applied to individual grid cells. The model was designed to be parsimonious rather than detailed, to support its use where there are few on-ground observations to force and constrain it, as is typical for Australia. Where possible, process equations were selected from the literature and through comparison against observations. The meteorological inputs are gridded daily total precipitation, incoming short-wave radiation, and minimum and maximum temperature, which are converted to daytime effective values {McVicar, 1999 #1040; van Dijk and Renzullo 2011}. Full technical details about the algorithms and default parameters can be found in the model technical documentation [(Van Dijk 2010b) (<http://eos.csiro.au/awra/>). In summary, the configuration considers two hydrological response units (HRUs): deep-rooted tall vegetation (“forest”) and shallow-rooted short vegetation (“herbaceous”), each of which occupies a fraction of each grid cell. Vertical processes are described for each HRU individually: (1) the net radiation balance, including incoming and outgoing short-wave and long-wave radiation and ground heat flux; (2) partitioning of precipitation between interception evaporation and net precipitation (van Dijk and Bruijnzeel 2001), and the partitioning of net precipitation between infiltration, infiltration excess surface runoff, and saturation excess runoff (van Dijk 2010c); (3) the water balance of three unsaturated soil layers (topsoil, shallow and deep soil layer) including infiltration, drainage (using equations derived from multilayer simulation studies) (Peeters et al. 2013), root water uptake (using a linear ramp function), and soil water evaporation; (4) transpiration, as the lesser of maximum root water uptake and optimum transpiration rate, estimated using the Penman-Monteith equation with aerodynamic conductance estimated from wind speed and maximum canopy conductance estimated from model leaf area and remotely sensed greenness (Yebra et al. 2013); (5) groundwater, surface water, and soil evaporation as a linear function of available energy (and for unsaturated soil, relative water content); (6) vegetation canopy dynamics (leaf biomass, canopy cover, leaf area index, and maximum canopy conductance) that adjust to balance actual and maximum transpiration with a degree of inertia corresponding to vegetation type. In addition, the following integrated catchment processes are described for each grid cell: (7) groundwater dynamics, including recharge from deep drainage, capillary rise (estimated with a linear diffusion equation), evaporation from groundwater saturated areas, and discharge (estimated with a linear reservoir model) (Peña-Arancibia et al. 2010; van Dijk 2010c); and (8) surface water body dynamics, including inflows from runoff and discharge, open water evaporation, and catchment water yield (estimated using a catchment-scale linear routing model) (van Dijk 2010c).

For the original model version 0.5 (Van Dijk 2010b), prior estimates of all HRU and catchment parameters were derived from the literature or data analysis. For version 1.0, 7 of the 34 parameters for each HRU and 2 catchment parameters were calibrated. The parameters included effective soil parameters determining hydraulic conductivity, water holding capacity and soil evaporation; relating remotely sensed greenness to maximum canopy conductance; and relating groundwater recession and saturated area to catchment characteristics. They were calibrated to optimize agreement with streamflow records from 160 small Australian catchments.

Some modifications of the AWRA-L version 1.0 model were needed for this application. Global data sets were used to configure the model, including tree cover fraction maps (Hansen et al. 2003), an albedo climatology derived from Moderate Resolution Imaging Spectroradiometer white-sky albedo (Moody et al. 2005) (<http://modis-atmos.gsfc.nasa.gov/ALBEDO/>) and a wind speed climatology (1983–1993) from NASA (<http://eosweb.larc.nasa.gov/sse/>). Australia experiences most major climate types (i.e., seasonal, arid, and humid; tropical, temperate, and cool), but significantly snowpack-affected catchments are few, and the model version used did not have a snow hydrology algorithm. Alternative approaches to including these processes were considered, varying from relatively simple conceptual approaches based on the temperature index or degree day concept (e.g. Lindström et al. 1997) to complex schemes based on explicit description of the energy balance of multiple snow layers (e.g. Cherkauer and Lettenmaier 1999). Previous assessments suggest that the increased complexity does not always lead to improved performance and makes greater demands on input data and calibration (Ferguson 1999). Therefore, in agreement with the overall parsimonious modelling philosophy, the simple but widely tested snow model used in HBV96 (Lindström et al. 1997) was implemented.

Runoff fields were propagated through a global routing scheme. Next, we used a global 0.5° resolution flow direction grid (Oki and Sud 1998; Oki et al. 2001) to parameterize a cell-to-cell river routing scheme. We used a linear reservoir kinematic wave approximation (Vörösmarty and Moore 1991), similar to that used in several large-scale hydrology models (see recent review by (Gong et al. 2011)). The routing function was an inverse linear function of the distance between network nodes and a transfer (or routing) coefficient. The resulting river flow estimates do not account for the impact of river water use (i.e., the evaporation of water extracted from rivers, mainly for irrigation).

4.10 WaterGAP3

The global water model WaterGAP3 (Water – Global Assessment and Prognosis) is a grid-based, integrative assessment tool to examine the state of global freshwater resources. The model framework consists of a spatially-distributed rainfall-runoff model, five sectorial water use models, and a large-scale water quality model.

The global hydrological model simulates the terrestrial part of the global hydrological cycle by a sequence of storage equations for the most relevant continental storage compartments: canopy, snowpack, soil, renewable groundwater, and surface water bodies. The model requires daily fields of precipitation, near-surface air temperature, downwelling shortwave and longwave radiation as external meteorological forcing. Potential evapotranspiration is estimated according to the Priestley-Taylor approach with surface net radiation calculated on the basis of land-cover dependent albedo and emissivity values.

The canopy storage is conceptualized as a single layer that intercepts precipitation until the maximum storage capacity is exceeded, and intercepted water evaporates at potential rate. Maximum canopy storage depends on daily LAI which is modelled as a function of land use dependent maximum LAI, fraction of deciduous plants and climate.

Snow accumulation and melt are simulated on a 1 arc minute sub-grid following a degree-day approach based on land-cover specific melting rates. Surface air temperature is disaggregated from 5 to 1 arc minute according to the elevation difference between each 5 arc minute cell and its corresponding sub-grid cells.

The soil column is represented as a single layer whose storage capacity is determined as a function of the soil texture dependent available water capacity (derived from soil maps) and the land-cover specific rooting depth. Total runoff from land is a function of effective precipitation, soil saturation, a non-linearity parameter and the fraction of urban area. The remaining part (effective precipitation minus runoff from land) is passed as infiltration to the soil storage. Groundwater recharge is calculated as a function of slope, soil texture, aquifer type, and the occurrence of permafrost/glaciers. Renewable groundwater resources are represented as a linear storage whose outflow is passed as subsurface runoff to the routing scheme.

Surface and subsurface runoff generated in each grid cell and inflow from upstream cells is transported through a series of linear and nonlinear retention storages representing lakes, reservoirs, and wetlands before contributing to streamflow. Flow velocity in the river segment is calculated as a function of river bed roughness, river bed slope and hydraulic radius of the channel according to the Manning-Strickler equation (Verzano et al. 2012). Lateral flow, i.e. between grid cells, is assumed to occur as streamflow only.

WaterGAP3 is calibrated in a basin-specific manner against long-term mean discharge by adjusting a runoff-nonlinearity parameter in each basin. In basins where adjusting this parameter does not provide an acceptable runoff estimate, i.e. the deviation from observed discharge remains larger than $\pm 1\%$, an additional runoff correction factor is assigned to each cell within the basin (same value for each cell). This correction factor effects all water balance components; if simulated discharge is too low, runoff will be increased and evaporation will be reduced and vice versa. This procedure is aimed to ensure a closed water balance, hence mass conservation, within the individual basin.

WaterGAP3 is explicitly designed to account for human interference on the natural streamflow regime through water abstraction and flow regulation by large dams and reservoirs. Spatially explicit time series of water withdrawal and water consumption are provided by the WaterGAP3 water use models (aus der Beek et al. 2010; Flörke et al. 2013) for five sectors: Domestic use (households and small businesses), manufacturing industries, thermal power plant cooling, irrigated agriculture and livestock farming. Sectorial water demands can be abstracted from surface water (rivers, reservoirs and lakes) and groundwater resources. Water demands for thermoelectric power plant cooling and livestock farming are assumed to be exclusively abstracted from surface water. For the remaining sectors, water withdrawals are allocated to groundwater and surface water abstractions according to sector- and cell-specific temporally constant groundwater use fractions derived from national and sub-national statistics (Döll et al. 2012).

The regulating effect of reservoirs on river discharge is simulated by a two-purpose operation scheme distinguishing irrigation and non-irrigation reservoirs (Döll et al. 2009). Operating rules are set individually for each reservoir as a function of mean annual inflow and water demand in lower reaches. Non-irrigation reservoirs are operated with the objective of providing constant release throughout the year. In the case of irrigation reservoirs, monthly release is additionally governed by downstream water demand, i.e. the cumulative monthly net abstraction in the next 20 downstream grid cells.

The WaterGAP3 simulations were carried out at 5 by 5 arc minute horizontal spacing. Storage compartments were initialized by re-running the first year of available meteorological forcing (1979) ten times. In a final step, simulated daily states and fluxes were scaled from the native 5 arc minute model resolution to 0.5° WRR-tier 1 resolution through area-weighted arithmetic averaging and summation, respectively.

5 Data

5.1 Data access

The simulations are available on the threads server and can be explored from: <https://wci.earth2observe.eu/thredds/catalog.html>. The list of available variables and direct http (follow the link in the table to a direct download of the file) and OPENDaP links is provided in Table 5.1 for the daily data. On the project github repository⁵, several scripts are available to download and spatially/temporally sample the data⁶. The appendix A provides an example of exploring and accessing the data in the server.

Table 5.1: Overview of daily simulations (and fixed fields) available in the data server. url and dap contain the direct http download link and the OPENDaP link (remove “.html” for applications access), respectively and NA when the variable is not available.

Variable	ecmwf	univu	metfr	nerc	jrc	cnrs	univk	csiro	eth
Precip	url,dap	url,dap	url,dap	url,dap	url,dap	url,dap	url,dap	url,dap	url,dap
Evap	url,dap	url,dap	url,dap	url,dap	url,dap	url,dap	url,dap	url,dap	url,dap
Runoff	url,dap	url,dap	url,dap	url,dap	url,dap	url,dap	url,dap	url,dap	url,dap
SWE	url,dap	url,dap	url,dap	url,dap	url,dap	url,dap	url,dap	url,dap	url,dap
SurfMoist	url,dap	url,dap	url,dap	url,dap	url,dap	NA	NA	NA	NA
RootMoist	url,dap	url,dap	url,dap	url,dap	url,dap	url,dap	url,dap	url,dap	NA
TotMoist	url,dap	url,dap	url,dap	url,dap	url,dap	url,dap	NA	url,dap	url,dap
Rainf	url,dap	url,dap	url,dap	url,dap	NA	url,dap	NA	NA	NA
Qs	url,dap	url,dap	url,dap	url,dap	url,dap	url,dap	url,dap	url,dap	NA
Qsb	url,dap	url,dap	url,dap	url,dap	url,dap	url,dap	url,dap	url,dap	NA
Qrec	NA	NA	NA	NA	NA	url,dap	NA	NA	NA
Qsm	url,dap	url,dap	url,dap	url,dap	url,dap	url,dap	url,dap	NA	NA
PotEvap	NA	url,dap	NA	NA	NA	url,dap	url,dap	url,dap	NA
ECanop	url,dap	url,dap	url,dap	url,dap	url,dap	url,dap	NA	url,dap	NA
TVeg	url,dap	url,dap	url,dap	NA	url,dap	url,dap	NA	url,dap	NA
ESoil	url,dap	url,dap	url,dap	NA	url,dap	url,dap	NA	url,dap	NA
EWater	NA	url,dap	NA	NA	url,dap	url,dap	NA	url,dap	NA
RivOut	url,dap	url,dap	url,dap	NA	url,dap	url,dap	url,dap	url,dap	NA
SWnet	url,dap	NA	url,dap	url,dap	NA	url,dap	NA	NA	NA
LWnet	url,dap	NA	url,dap	url,dap	NA	url,dap	NA	NA	NA
Qle	url,dap	NA	url,dap	url,dap	NA	url,dap	NA	NA	NA
Qh	url,dap	NA	url,dap	url,dap	NA	url,dap	NA	NA	NA
AvgSurfT	url,dap	NA	url,dap	url,dap	NA	url,dap	NA	NA	NA
Albedo	url,dap	NA	url,dap	url,dap	NA	url,dap	url,dap	url,dap	NA
LAI	url,dap	NA	url,dap	url,dap	NA	NA	url,dap	url,dap	NA
CanopInt	url,dap	url,dap	url,dap	url,dap	NA	NA	url,dap	NA	NA
SWEVeg	NA	NA	NA	url,dap	NA	NA	NA	NA	NA
SurfStor	NA	url,dap	url,dap	NA	NA	url,dap	url,dap	NA	NA
WaterTableD	NA	NA	NA	NA	NA	NA	NA	NA	NA
SnowFrac	url,dap	NA	url,dap	url,dap	NA	url,dap	url,dap	url,dap	NA
SnowDepth	url,dap	NA	url,dap	url,dap	NA	url,dap	NA	NA	NA
GroundMoist	NA	url,dap	url,dap	NA	url,dap	NA	NA	url,dap	NA
lsm	url,dap	url,dap	url,dap	url,dap	NA	NA	NA	NA	NA

⁵ <https://github.com/earth2observe/project-tools>

⁶ <https://github.com/earth2observe/project-tools/tree/master/data-access-examples>

Variable	ecmwf	univu	metfr	nerc	jrc	cnrs	univk	csiro	eth
SurfSoilSat	url,dap	url,dap	url,dap	url,dap	url,dap	NA	NA	NA	NA
RootSoilSat	url,dap	url,dap	url,dap	url,dap	url,dap	NA	NA	NA	NA
TotSoilSat	url,dap	NA	url,dap	url,dap	url,dap	NA	NA	NA	NA

5.2 Metadata and quality control

Two quality control tests were applied to the data: (i) generic metadata and quality control; (2) comparison of minimum, maximum and mean fields. The first test is automatic, while the second relies on the visual inspection of the plots.

The scripts used for the generic meta-data and quality control are available in the project github repository⁷. The checks are performed to:

1. File consistency checks:
 - a. If a file is not found it is reported as a warning;
 - b. File name consistency;
 - c. Variable attributes;
 - d. File coordinates consistency.
2. Evaluation of energy balance (for the models that provide the needed variables)
 - a. Computes the net energy as:
 - i. $SW_{net} + LW_{net} + Q_{le} + Q_h = \text{residual}$.
3. Evaluation and closure of grid-point water balance:
 - a. The water balance in each grid point:
 - i. $Precip + Runoff + Evap = \Delta(SWE + SoilMoist, GroundMoist, SurfStor, CanopInt)$
 - ii. Averaged over the full period the two terms of the equation should balance within $5 \times 10^{-6} \text{ kg m}^{-2} \text{ s}^{-1}$
4. Computation of global land means of the different fluxes for consistency checks (e.g. fluxes signal conventions).

All data that passed the meta-data consistency checks, and the water balance residual are displayed in the appendix B (Figure 9.1). The simulations from univk, univu, jrc, cnrs and nerc have grid-points with residuals above the defined threshold due the water transport in the river network that is not accounted for in the water balance calculations, but the water balance is closed on a regional scale. The eth simulations should not be considered over glacier regions (Greenland, Antarctica) due to limitations of the SWBM in representing snow evolution in those areas. The jrc water balance residuals did not account for precipitation as it was available on the data server.

For the second data quality check, the temporal and field minimum, maximum, mean and standard deviation was computed for all variables and compared among the different models using the monthly means data. This allowed the identification of several problems (e.g. different signal conventions for the fluxes, numerical/rounding errors, etc...) that were corrected directly in the data server or by each institution. The examples in Figure 9.2 to Figure 9.11 illustrate the spread of the different models for selected variables. The following points describe known issues of the dataset that are due to model assumptions and were detected during the quality control:

⁷ <https://github.com/earth2observe/project-tools/tree/master/Quality-Control-for-Model-Output>

- Univk simulations report large values of evaporation in some grid points (see Figure 9.3) that are due to the allocation of the evaporation of large lakes to the grid points that represent the outlet of these lakes.
- Jrc simulations of SurfMoist report comparably high values (Figure 9.7) that are due assigning the top layer soil moisture as SurfMoist.
- Jrc simulations of GroundMoist (Figure 9.10) can have below zero values if water use exceeds recharge.
- Metfr simulations of RootMoist and TotMoist (Figure 9.8 and Figure 9.9) contain comparably high values that are due to the soil depth and texture specifications.
- All model simulations of SWE (Figure 9.11) report very large values that are located over Greenland and Antarctica. Since any of the models have a specific representation of glaciers, we recommend that SWE should not be used over those areas.

6 Inter-comparison

A detailed evaluation of the dataset is an independent task in the project and in this section we intend to demonstrate the usability of the data in the server by inter-comparing the different model simulations in terms of multi-model estimates and also some examples of verification.

6.1 Multi-model

In this section we present the multi-model mean and standard deviation of a selected number of variables (the individual maps for each model is available in the appendix B in Figure 9.12 to Figure 9.16). The purpose of this comparison is twofold: (i) evaluate the quality of the model simulations and (ii) demonstrate the use and potential of the multi-model estimates.

The large evaporation and runoff rates in the tropics are consistent among all models along with an associated large RootMoisture. In these regions, the large multi-model mean fluxes are also associated with a larger inter-model variability that is likely associated with the different treatment of evaporation and soil hydrology among the models. In the RootMoist, we can also identify a region of large inter-model variability in the Northern Latitudes that is associated with the different snow melting rates among the models, and is consistent with the snow mass distribution. In the snow mass distribution, there are two regions (i) Eastern Canadian Shield and (ii) between the Ural Mountains and the Central Siberian Plateau with a high inter-model variability that might be linked with differences in the land cover types among the models. Finally, the TotMoist multi-model mean and standard deviation display a large range of values with a clear geographic signal poleward 50° N with higher soil moisture content and variability that is mainly associated with the particular fields of metfr simulations (see Figure 9.16).

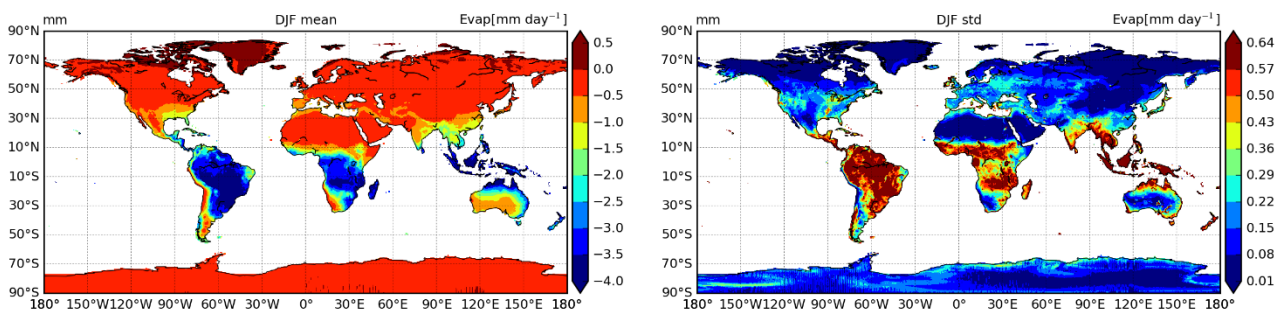


Figure 6.1: Multi-model mean (left) and standard deviation (right) of northern hemisphere winter evaporation.

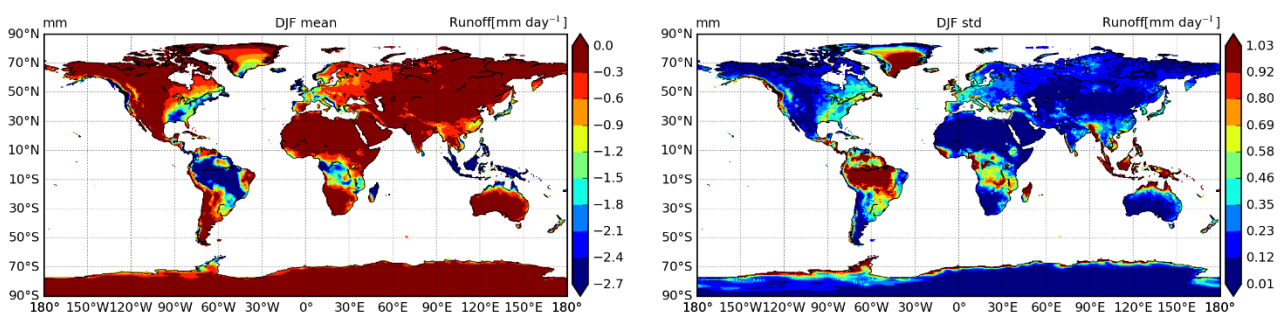


Figure 6.2: Multi-model mean (left) and standard deviation (right) of northern hemisphere winter Runoff.

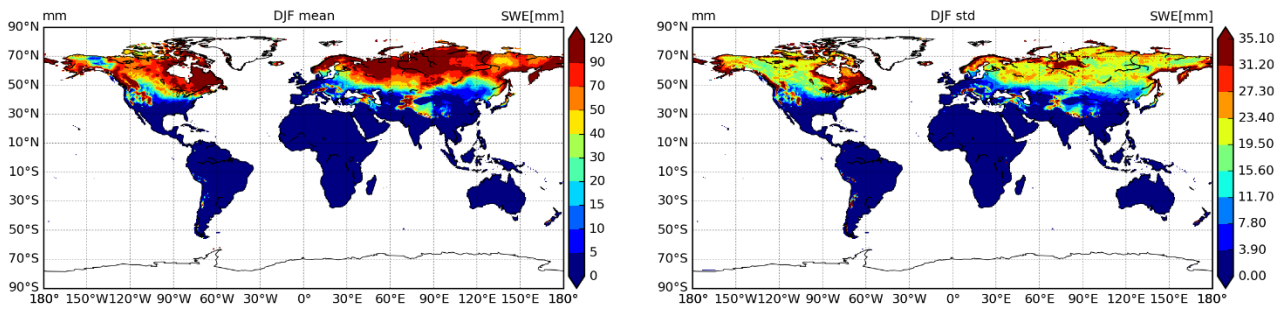


Figure 6.3: Multi-model mean (left) and standard deviation (right) of northern hemisphere winter SWE. Values above 500 mm (both for the mean and standard deviation) are masked to screen Greenland and Antarctica.

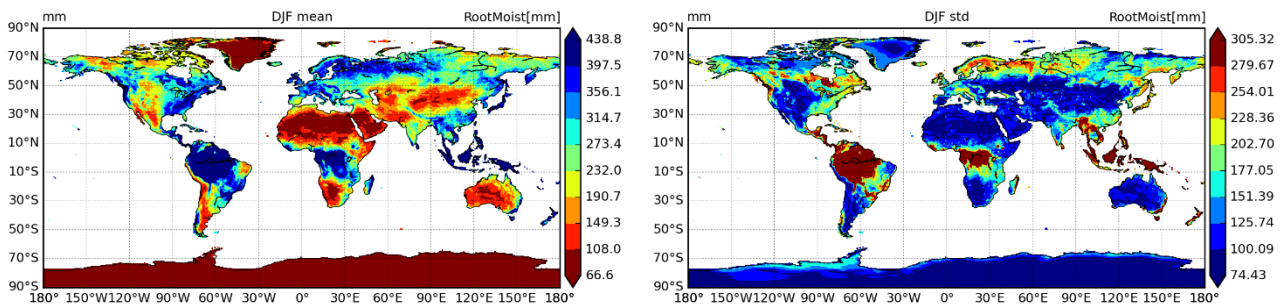


Figure 6.4: Multi-model mean (left) and standard deviation (right) of northern hemisphere winter RootMoist.

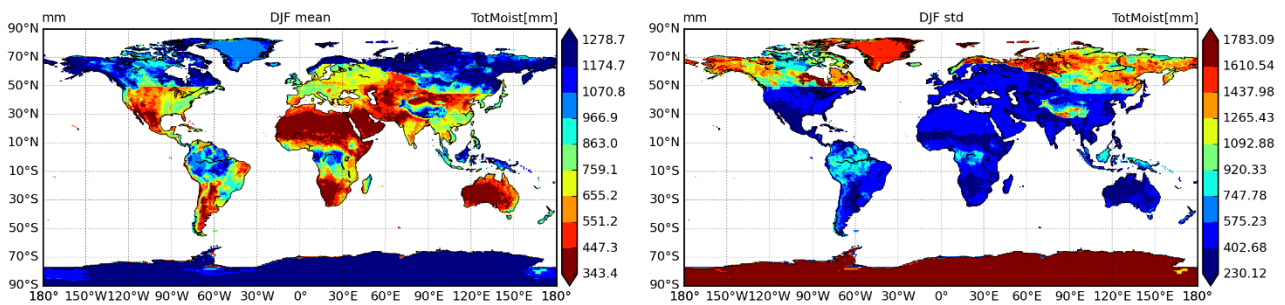


Figure 6.5: Multi-model mean (left) and standard deviation (right) of northern hemisphere winter TotMoist.

6.2 Verification examples

Figure 6.6 presents an example of comparing the mean northern hemisphere winter snow cover fraction from the Interactive Multisensor Snow and Ice Mapping System (IMS) with the multi-model model. The specific model fields and biases are provided in the appendix B (see Figure 9.18). There is a general under-estimation of snow cover in the surroundings of the snow line. This can be partially explained by the binary nature of the IMS datasets - Snow/No snow that was spatially aggregated to the 0.5x0.5 grid. The IMS reports snow when there is at least 50% of the 4km pixel covered with snow. Therefore, the IMS provides the upper limit of snow cover fraction, and negative biases in the models must be carefully evaluated. Apart from the general under-estimation we can identify two main features in the multi-model: (i) overestimation over the Western/Central Tibetan plateau and (ii) underestimation over the Canadian Shield near Hudson Bay and near the Canada/Alaska border. In the first case, the multi-model standard deviation is small suggesting that this could be either a problem in the forcing or in the observations, while in the second case there is a large model spread (that can be confirmed in each model bias in Figure 9.18) suggesting other problems representing snow cover in

those regions. This comparison provides a simple example of the use of the multi-model mean and spread to identify systematic problems in the dataset.

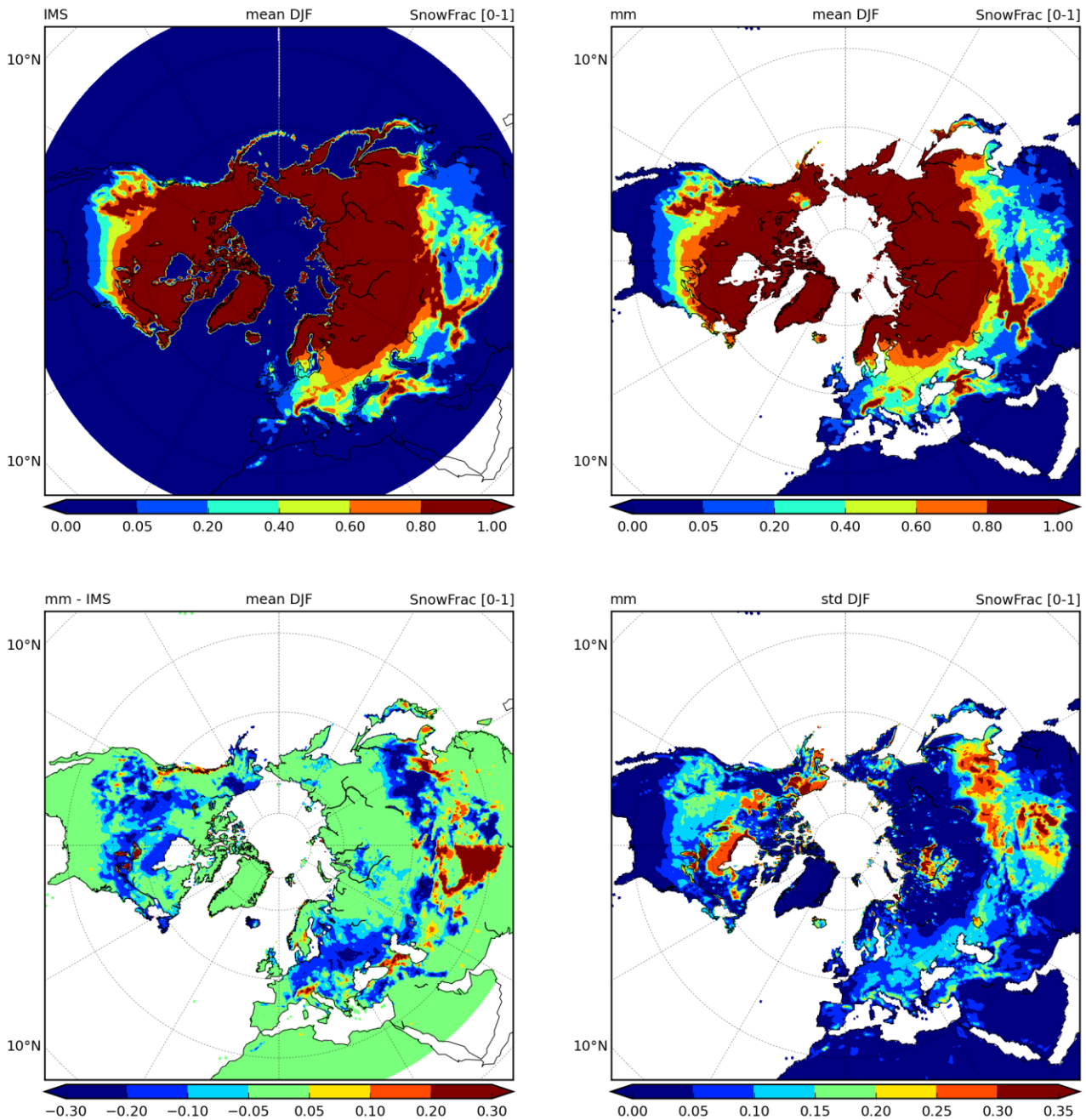


Figure 6.6: Mean northern hemisphere winter snow cover fraction in the IMS dataset (top left) compared with the multi-model (MM) mean (top right) and the mean difference between MM-IMS (bottom left) and the MM standard deviation (bottom right).

Simulated terrestrial water storage variations (ΔTWS) can be estimated by GRACE products. GRACE provides monthly anomalies based on highly accurate maps of the Earth's gravity fields over spatial scales about 300km since 2002. 3 GRACE products exist (from GFZ, CSR and JPL) and the standard deviation and mean of the 3 products are generally used as reference. The monthly TWS variations simulated by a hydrological model are calculated as the sum of the total soil moisture, the snow cover equivalent, the vegetation interception, the stream water content and the groundwater reservoir.

Figure 6.7 represents an example of validation for the simulated TWS. The climatological Δ TWS provided by GRACE (left), simulated by SURFEX (center) and their zonal average (right) are represented.

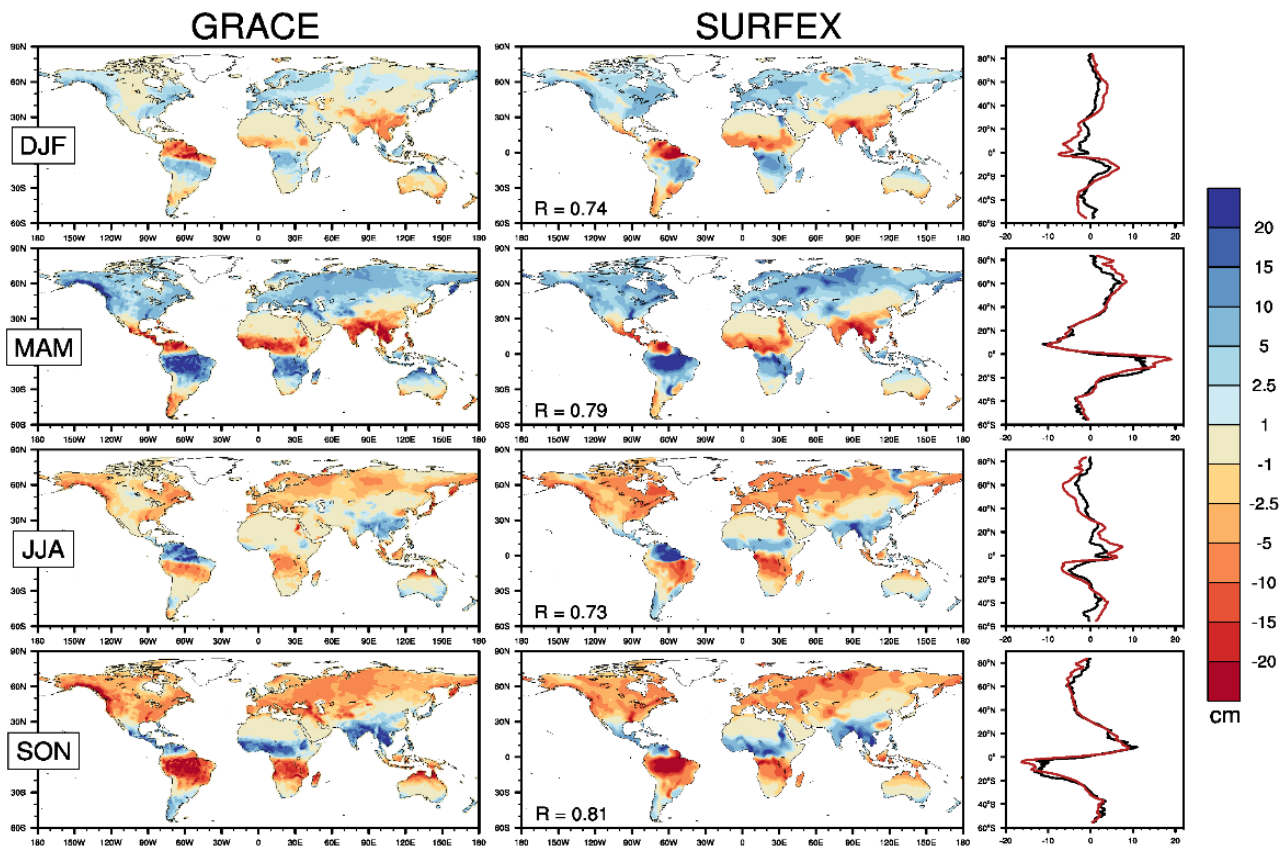


Figure 6.7: Climatological comparison of observed Δ TWS (mean GRACE product, left column) and simulated with SURFEX (center) for DJF, MAM, JJA and SON over the 2002-2012 period. The spatial correlation between GRACE and SURFEX climatologies are indicated for each season on the SURFEX maps. Right column, the zonal average of Δ TWS for GRACE (black line) and SURFEX (red).

7 Summary

The first version of the water resources reanalysis produced by 10 different models has been compiled and is available in the data server. This report describes the modelling protocol, and different modelling systems. Special attention has been given to the harmonization of the different model outputs into a common netcdf4 standard following the CF conventions, as well as to the use of a standard file naming convention and location on the data server. The dataset was screened for general meta-data and quality problems, and all problems found were corrected. A particular focus was given to the data access presenting several examples and software that is available in the project github space⁸.

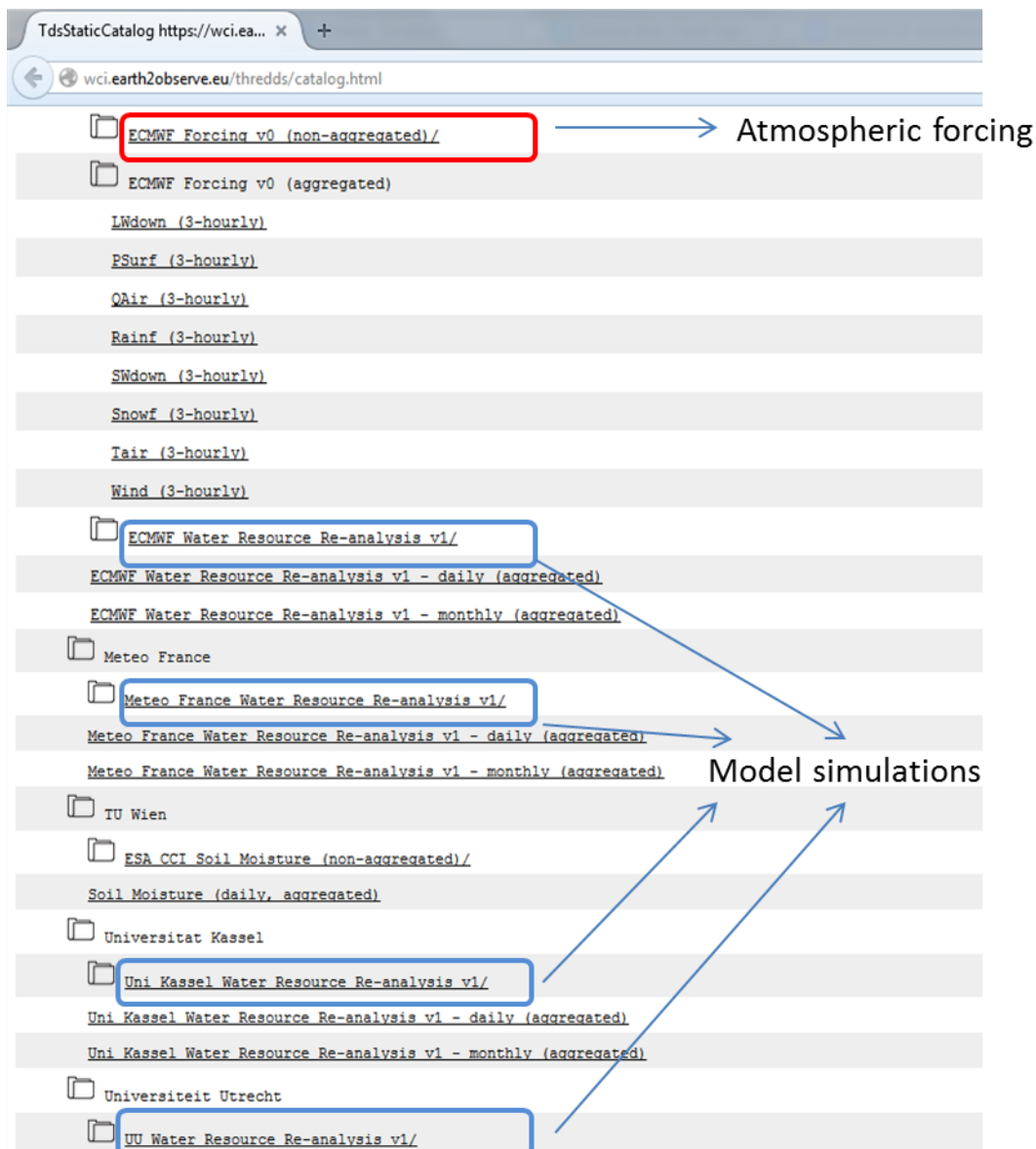
⁸ <https://github.com/earth2observe/project-tools>

8 Appendix A – Data server access example

The following steps illustrate an interactive navigation in the data server using a web browser. This can be used to find data, to download specific files or to find the files location for later use in automatic scripts (see example in linux : https://github.com/earth2observe/project-tools/blob/master/data-access-examples/extract_E2OBS_simulations.ksh).

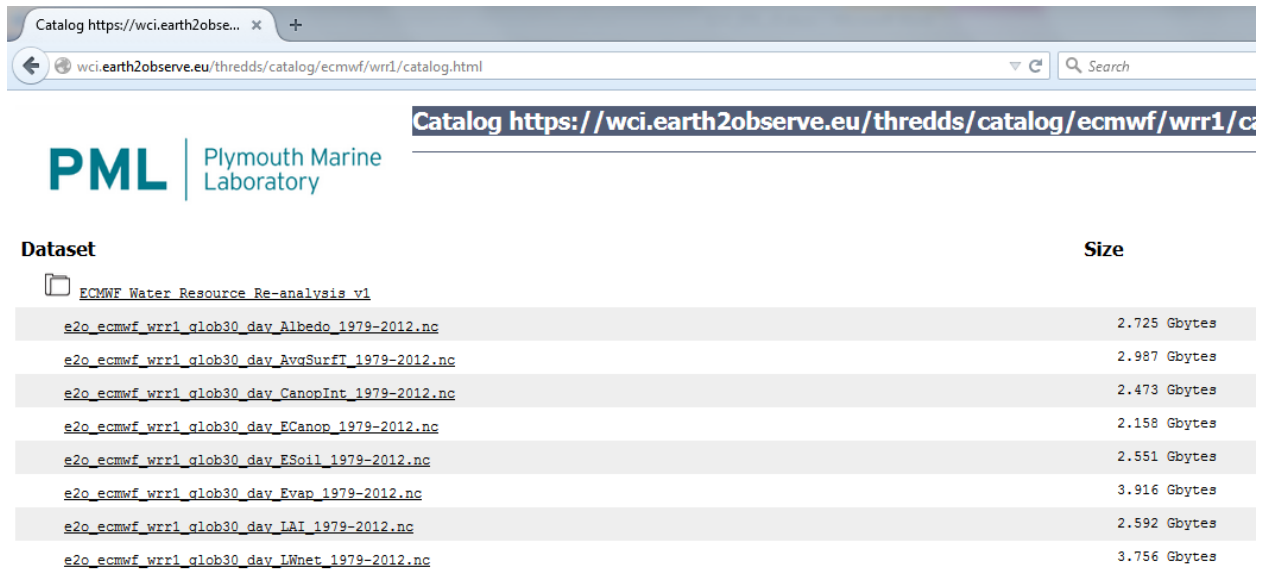
A list of software that can be used to explore and display netcdf data can be found at: <http://www.unidata.ucar.edu/software/netcdf/software.html>

1. Go to the webpage: <http://wci.earth2observe.eu/thredds/catalog.html>



This catalog page contains all the project datasets (model simulations and observational datasets).

2. For a particular model simulation click on the link containing the model name and “Water Resources Re-analysis v1”.



Catalog <https://wci.earth2observe.eu/thredds/catalog/ecmwf/wrr1/catalog.html>

PML | Plymouth Marine Laboratory

Dataset	Size
ECMWF Water Resource Re-analysis v1	
e2o_ecmwf_wrr1_glob30_day_Albedo_1979-2012.nc	2.725 Gbytes
e2o_ecmwf_wrr1_glob30_day_AvgSurfT_1979-2012.nc	2.987 Gbytes
e2o_ecmwf_wrr1_glob30_day_CanopInt_1979-2012.nc	2.473 Gbytes
e2o_ecmwf_wrr1_glob30_day_ECanop_1979-2012.nc	2.158 Gbytes
e2o_ecmwf_wrr1_glob30_day_ESoil_1979-2012.nc	2.551 Gbytes
e2o_ecmwf_wrr1_glob30_day_Evap_1979-2012.nc	3.916 Gbytes
e2o_ecmwf_wrr1_glob30_day_LAI_1979-2012.nc	2.592 Gbytes
e2o_ecmwf_wrr1_glob30_day_LWnet_1979-2012.nc	3.756 Gbytes

This page will display all the available variables for the specific model (in this case ecmwf/wrr1 – see the http url)

3. Select the file you want to explore



Catalog https://wci.earth2observe.eu/thredds/catalog/ecmwf/wrr1/catalog.html?dataset=ecmwf-wrr1/e2o_ecmwf_wrr1_g

Dataset: ECMWF Water Resource Re-analysis v1/e2o_ecmwf_wrr1_g

- Data size: 3.916 Gbytes
- Data type: GRID
- Naming Authority: ecmwf.int
- ID: ecmwf-wrr1/e2o_ecmwf_wrr1_glob30_day_Evap_1979-2012.nc

Documentation:

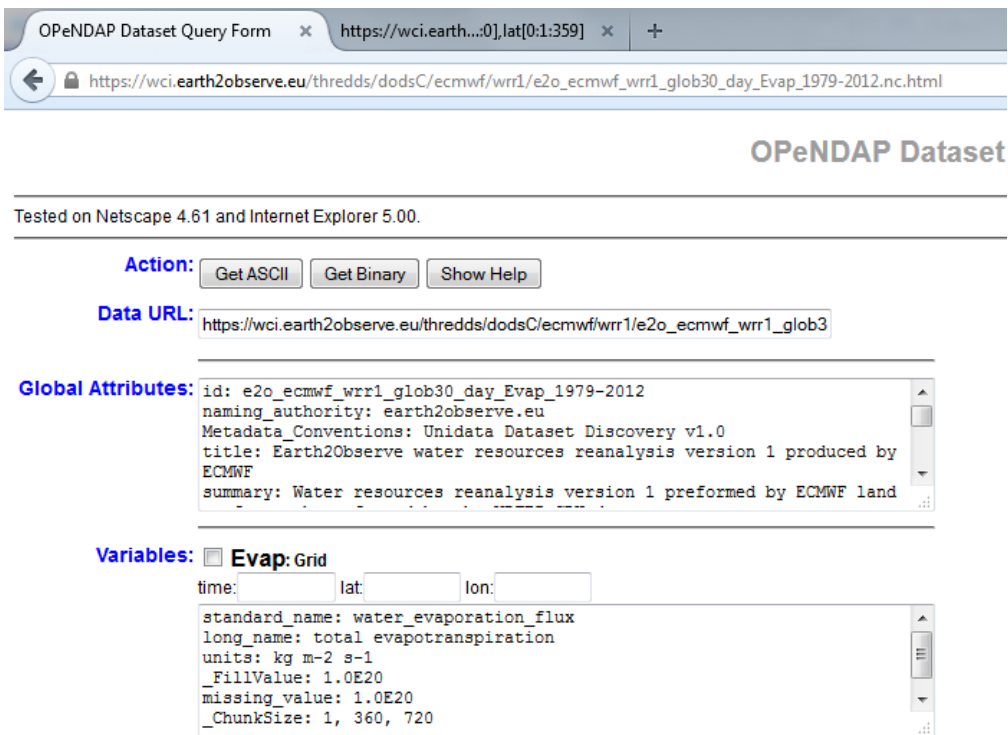
- **Summary:** WATCH forcing data methodology applied to ERA-Interim data
- **Rights:** These data can be used freely for research purposes provided that the following source is acknowledged: doi:10.1002/2014WR015638. This data is made available in the hope that it will be useful, but WITHOUT ANY WARRANTY.

Access:

1. **OPENDAP:** [/thredds/dodsC/ecmwf/wrr1/e2o_ecmwf_wrr1_glob30_day_Evap_1979-2012.nc](#)
2. **HTTP Server:** [/thredds/fileServer/ecmwf/wrr1/e2o_ecmwf_wrr1_glob30_day_Evap_1979-2012.nc](#)
3. **WCS:** [/thredds/wcs/ecmwf/wrr1/e2o_ecmwf_wrr1_glob30_day_Evap_1979-2012.nc](#)
4. **WMS:** [/thredds/wms/ecmwf/wrr1/e2o_ecmwf_wrr1_glob30_day_Evap_1979-2012.nc](#)
5. **NCML:** [/thredds/ncml/ecmwf/wrr1/e2o_ecmwf_wrr1_glob30_day_Evap_1979-2012.nc](#)
6. **Data discovery report:** [/thredds/uddc/ecmwf/wrr1/e2o_ecmwf_wrr1_glob30_day_Evap_1979-2012.nc](#)
7. **ISO19115/Inspire:** [/thredds/iso/ecmwf/wrr1/e2o_ecmwf_wrr1_glob30_day_Evap_1979-2012.nc](#)

4. For a direct download of the file click on the option 2: "HTTP Server"

5. To explore the header of the file select option 1: "OPENDAP"



The screenshot shows a web browser window with the following elements:

- Browser Tabs:** "OPeNDAP Dataset Query Form" and "https://wci.earth...0],lat[0:1:359]".
- Address Bar:** "https://wci.earth2observe.eu/thredds/dodsC/ecmwf/wrr1/e2o_ecmwf_wrr1_glob30_day_Evap_1979-2012.nc.html"
- Section Header:** "OPeNDAP Dataset"
- Compatibility Note:** "Tested on Netscape 4.61 and Internet Explorer 5.00."
- Action:** Buttons for "Get ASCII", "Get Binary", and "Show Help".
- Data URL:** "https://wci.earth2observe.eu/thredds/dodsC/ecmwf/wrr1/e2o_ecmwf_wrr1_glob30" (Note: the image shows a truncated URL).
- Global Attributes:**

```

id: e2o_ecmwf_wrr1_glob30_day_Evap_1979-2012
naming_authority: earth2observe.eu
Metadata_Conventions: Unidata Dataset Discovery v1.0
title: Earth2Observe water resources reanalysis version 1 produced by ECMWF
summary: Water resources reanalysis version 1 preformed by ECMWF land
            
```
- Variables:**
 - Evap: Grid**
 - time: lat: lon:
 - standard_name: water_evaporation_flux
 - long_name: total evapotranspiration
 - units: kg m⁻² s⁻¹
 - _FillValue: 1.0E20
 - missing_value: 1.0E20
 - _ChunkSize: 1, 360, 720

In this dataset explorer, you can find the variable attributes (e.g units), and download sub-sets of the file in “Get ASCII” or “Get Binary”.

9 Appendix B - Figures

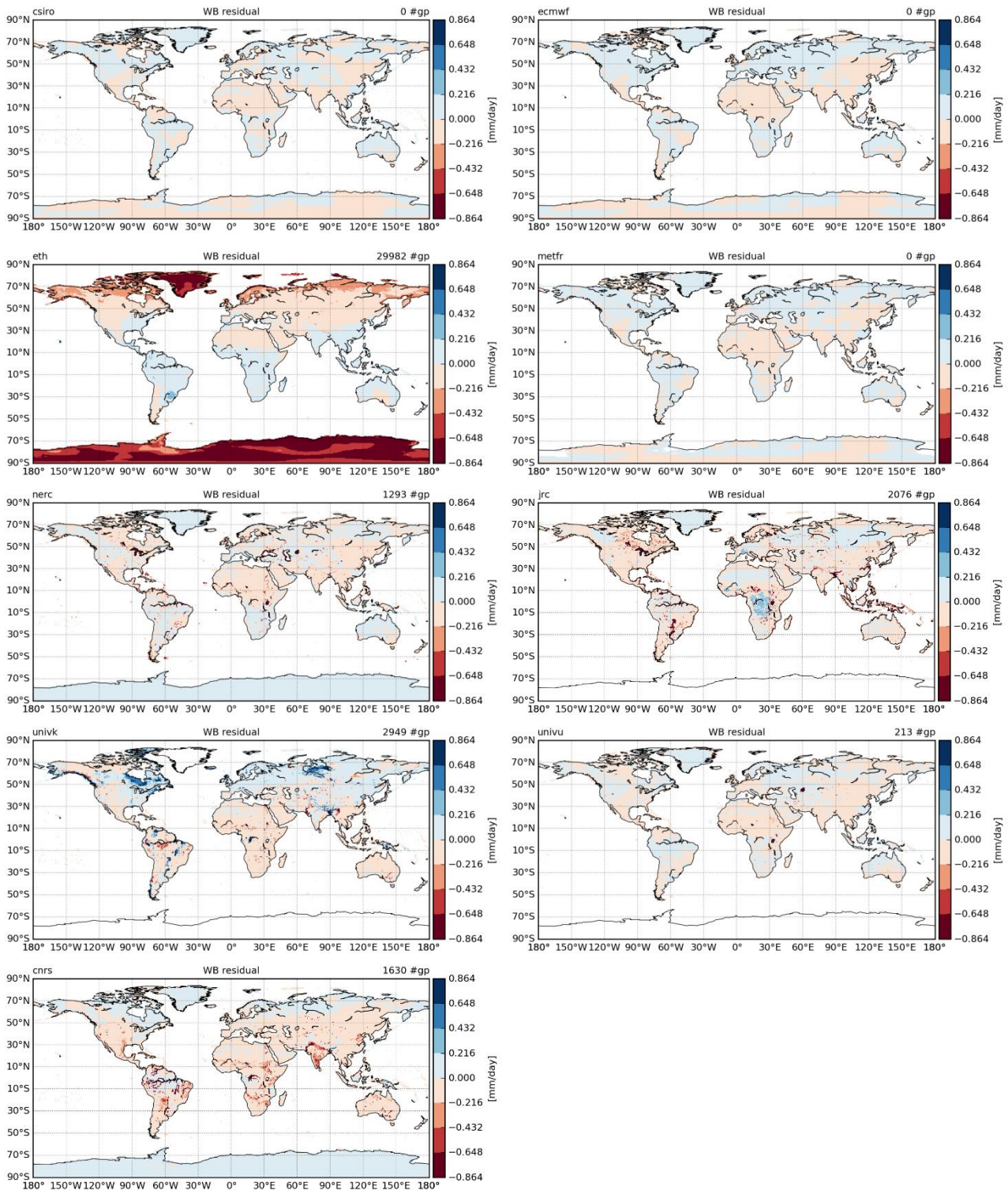


Figure 9.1: Water balance residual for each modelling system. The residual is calculated as the sum of the water fluxes plus the storage term changes between 1st January 1979 and the 31st December 2012. Residuals above ± 0.432 mm/day are assumed to be above the data precision.

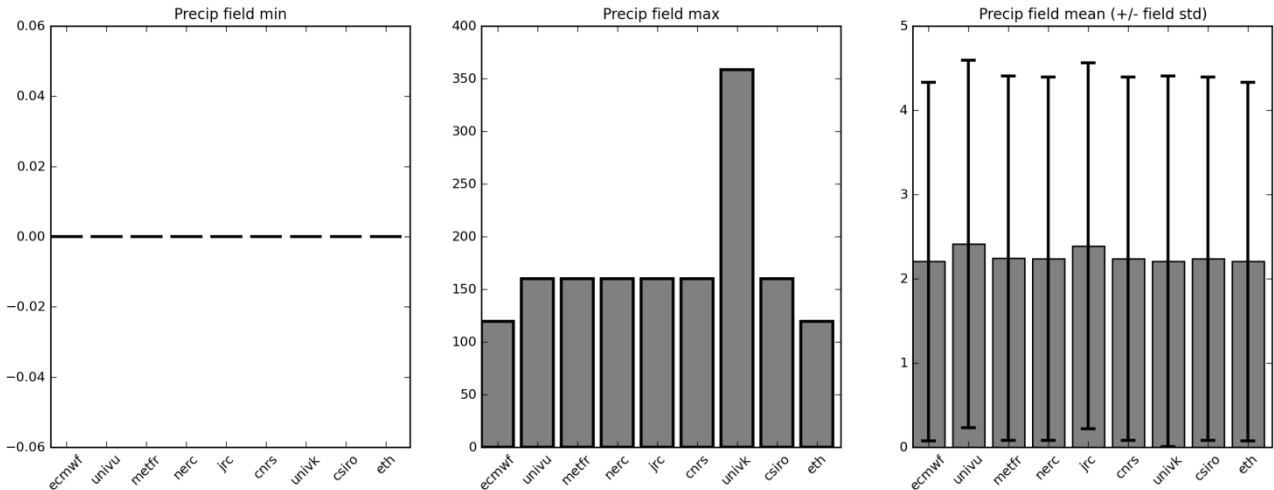


Figure 9.2: Statistics of the Precip (mm day⁻¹) simulations derived from the monthly means: (left) temporal and spatial minimum; (center) temporal and spatial maximum (right) temporal and spatial mean, with the error bars denoting the spatial standard deviation of the temporal mean. The red symbol indicates that the simulation for a particular model is not available.

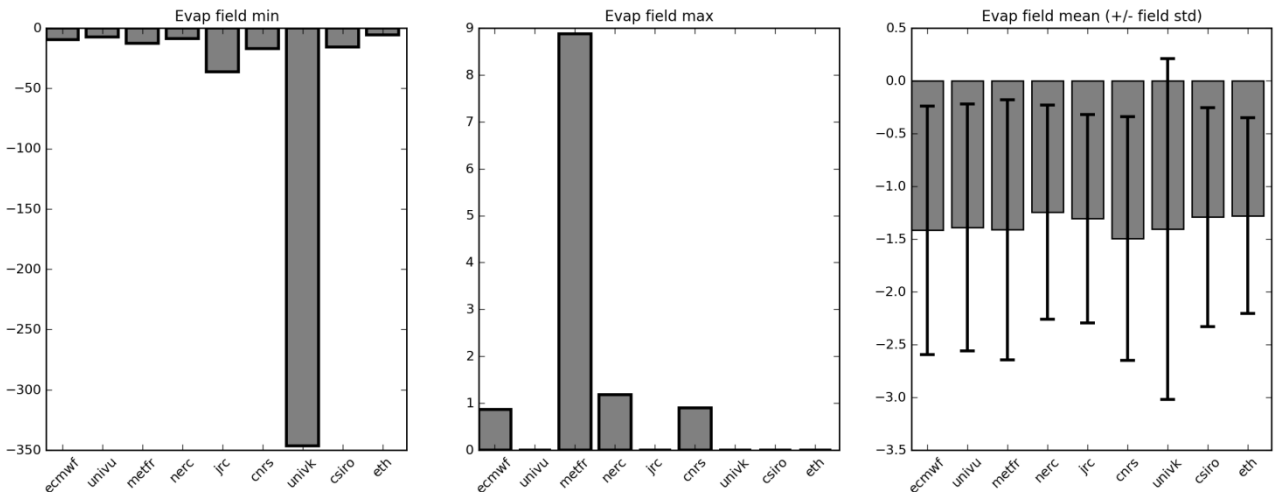


Figure 9.3: As Figure 9.2 but for Evap (mm day⁻¹).

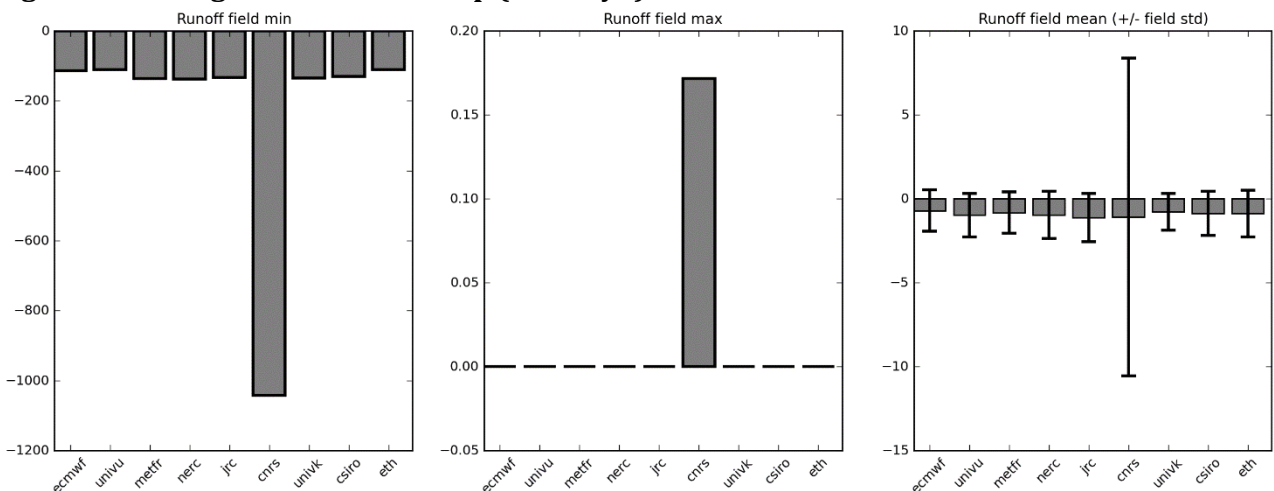


Figure 9.4: As Figure 9.2 but for Runoff (mm day⁻¹).

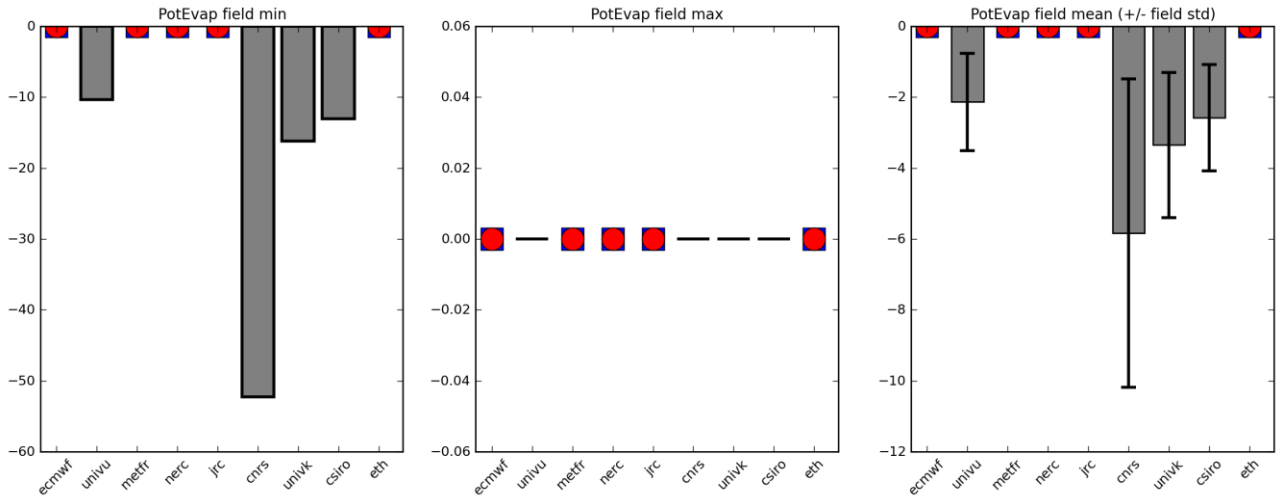


Figure 9.5: As Figure 9.2 but for PotEvap (mm day⁻¹).

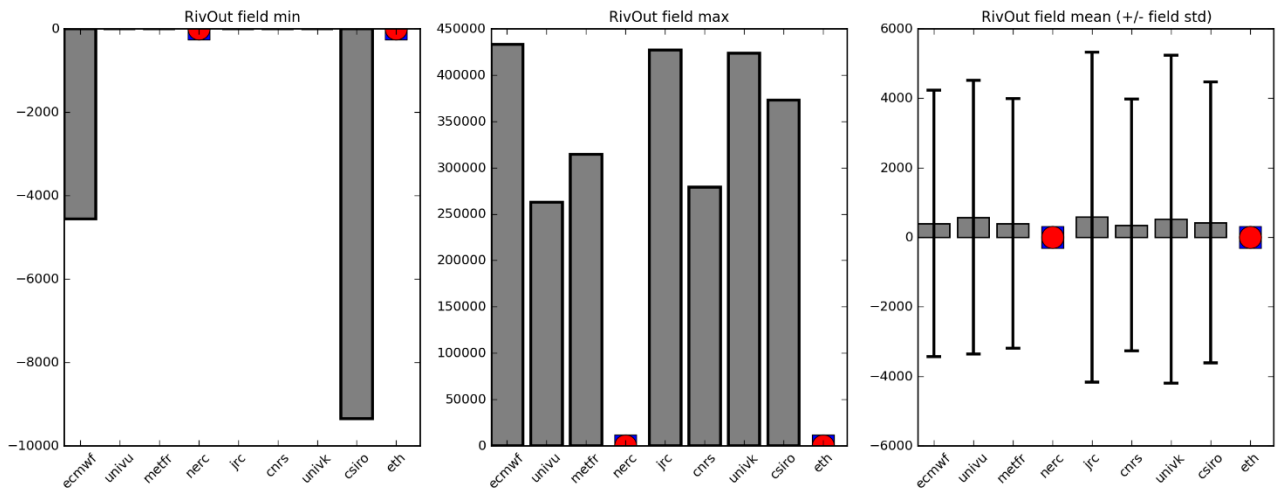


Figure 9.6: As Figure 9.2 but for RivOut (m³ s⁻¹).

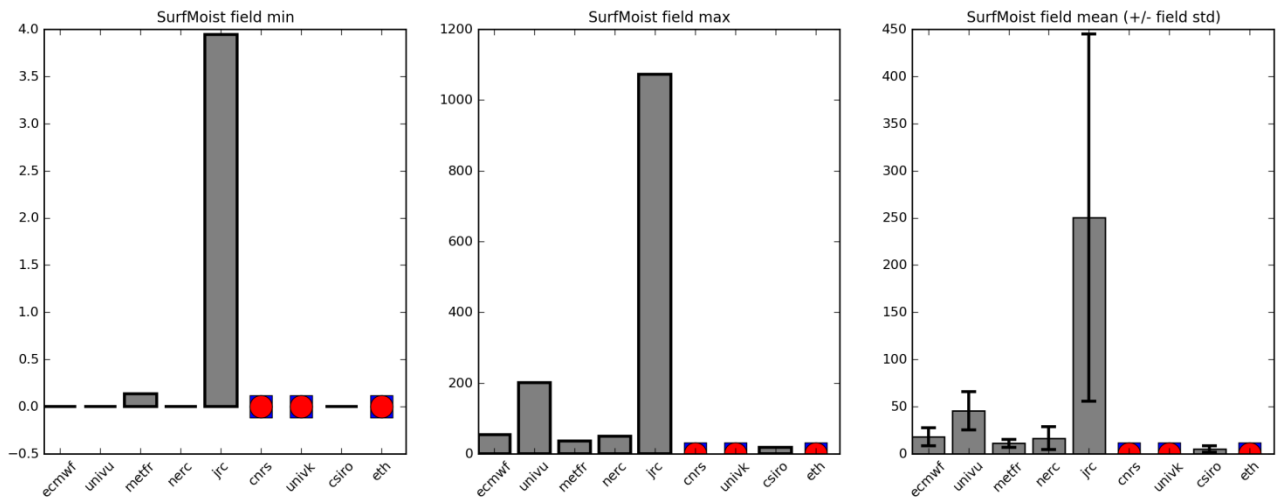


Figure 9.7: As Figure 9.2 but for the SurfMoist (kg m⁻²).

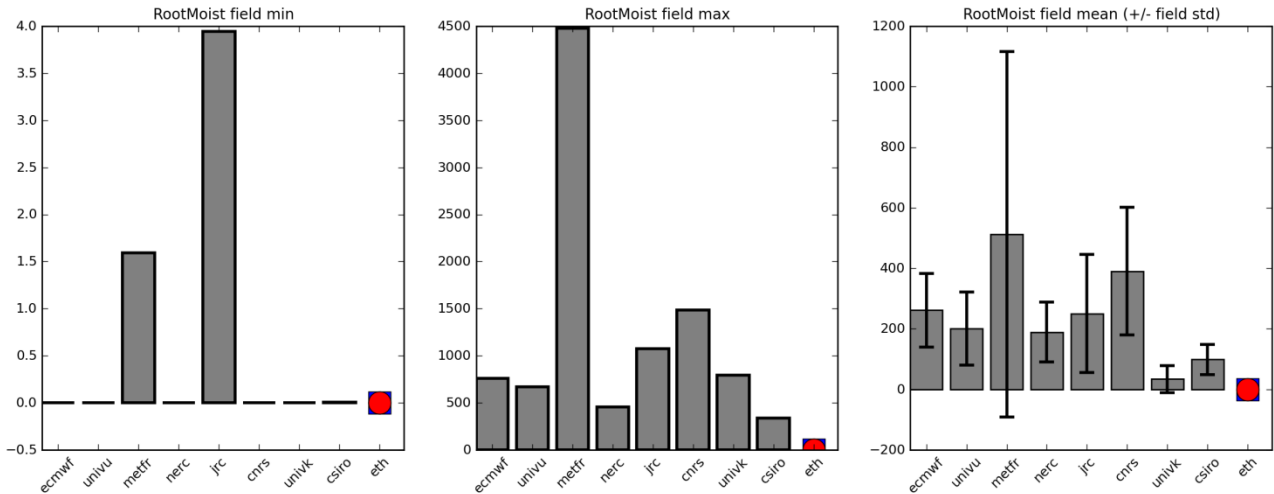


Figure 9.8: As Figure 9.2 but for the RootMoist (kg m⁻²).

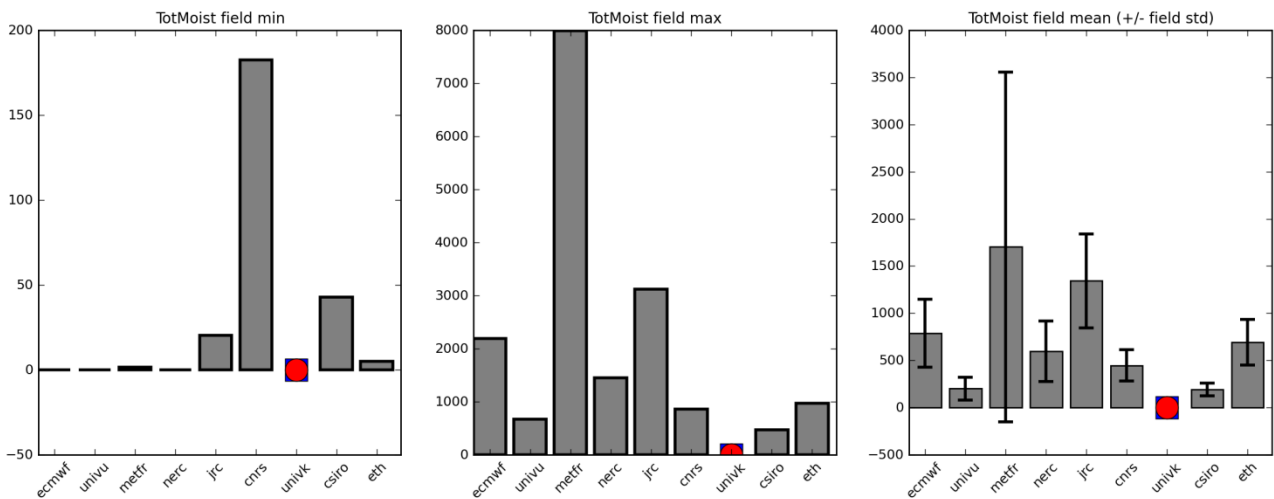


Figure 9.9: As Figure 9.2 but for the TotMoist (kg m⁻²).

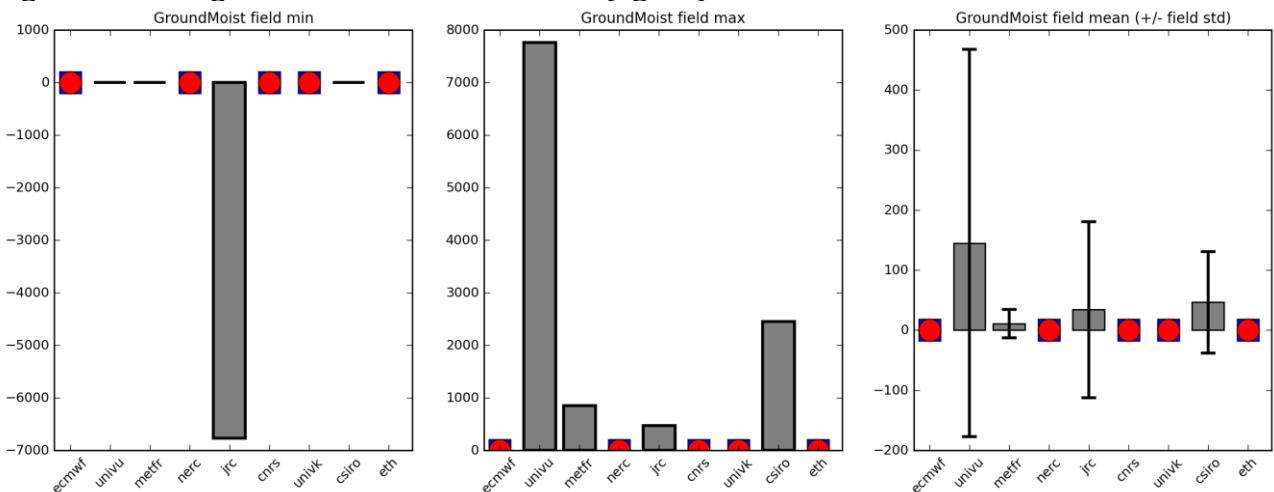


Figure 9.10: As Figure 9.2 but GroundMoist (kg m⁻²).

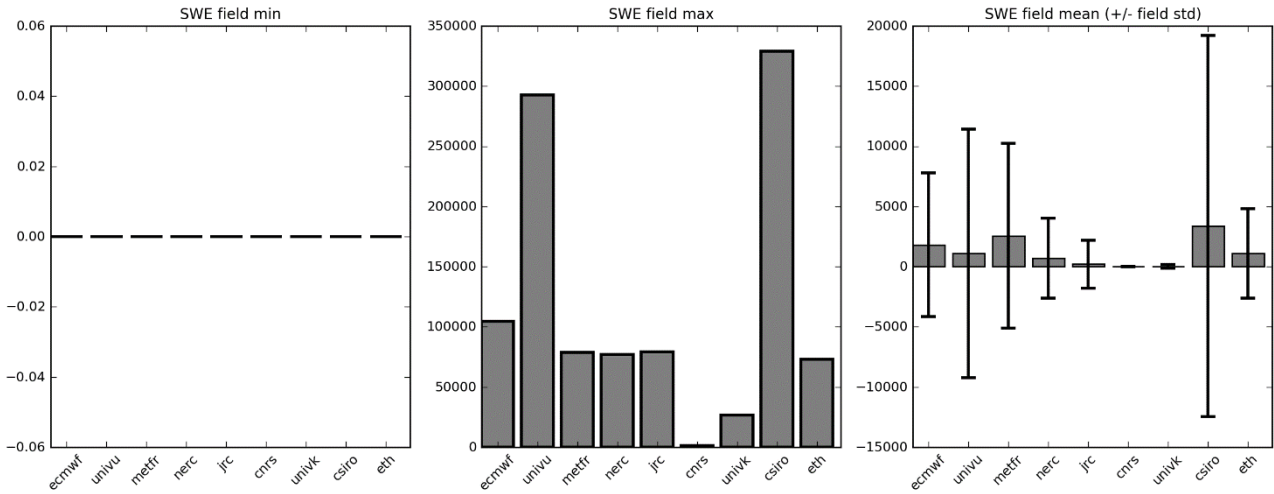


Figure 9.11: As Figure 9.2 but for the SWE (kg m⁻²).

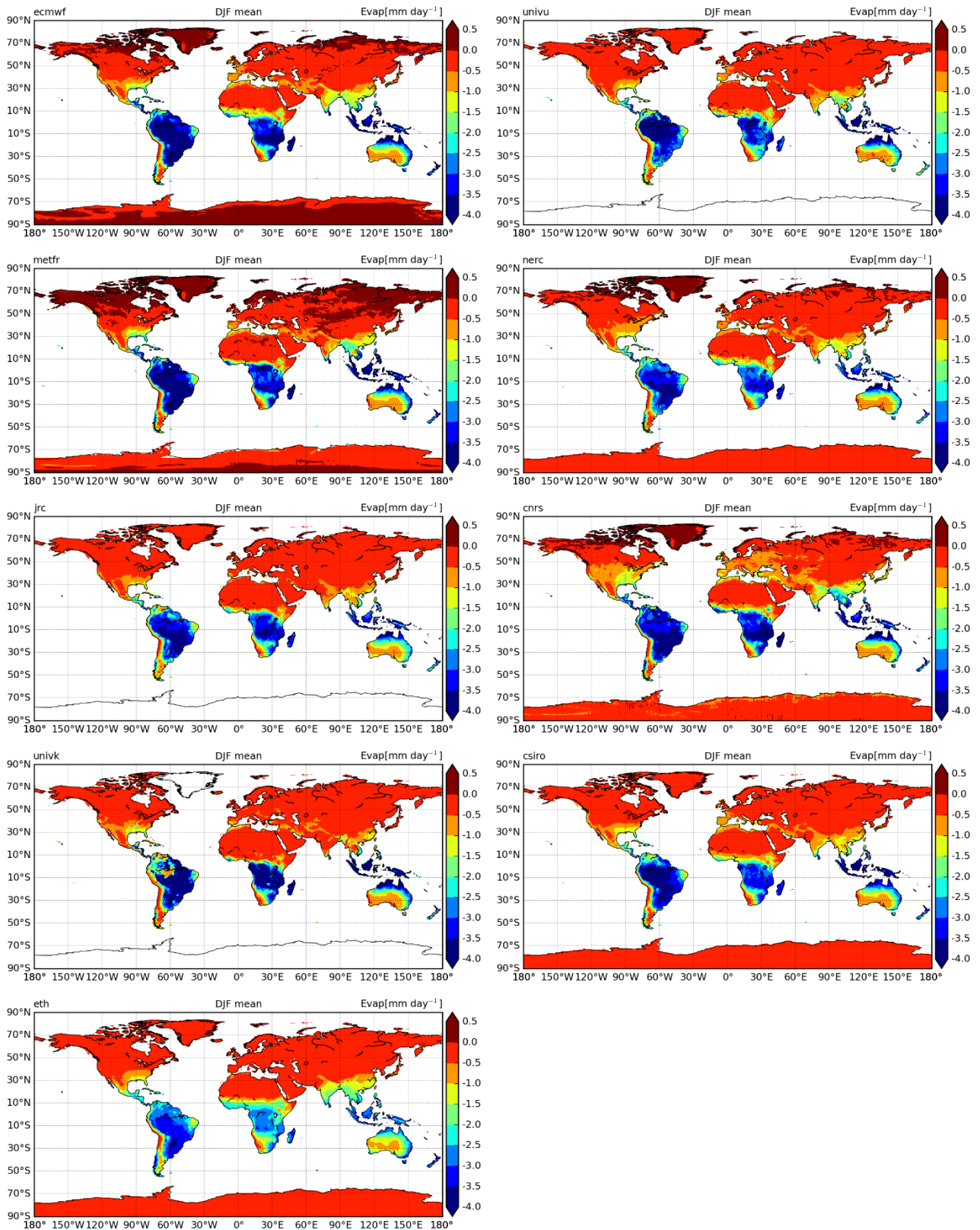


Figure 9.12: Mean northern hemisphere winter evaporation in each model.

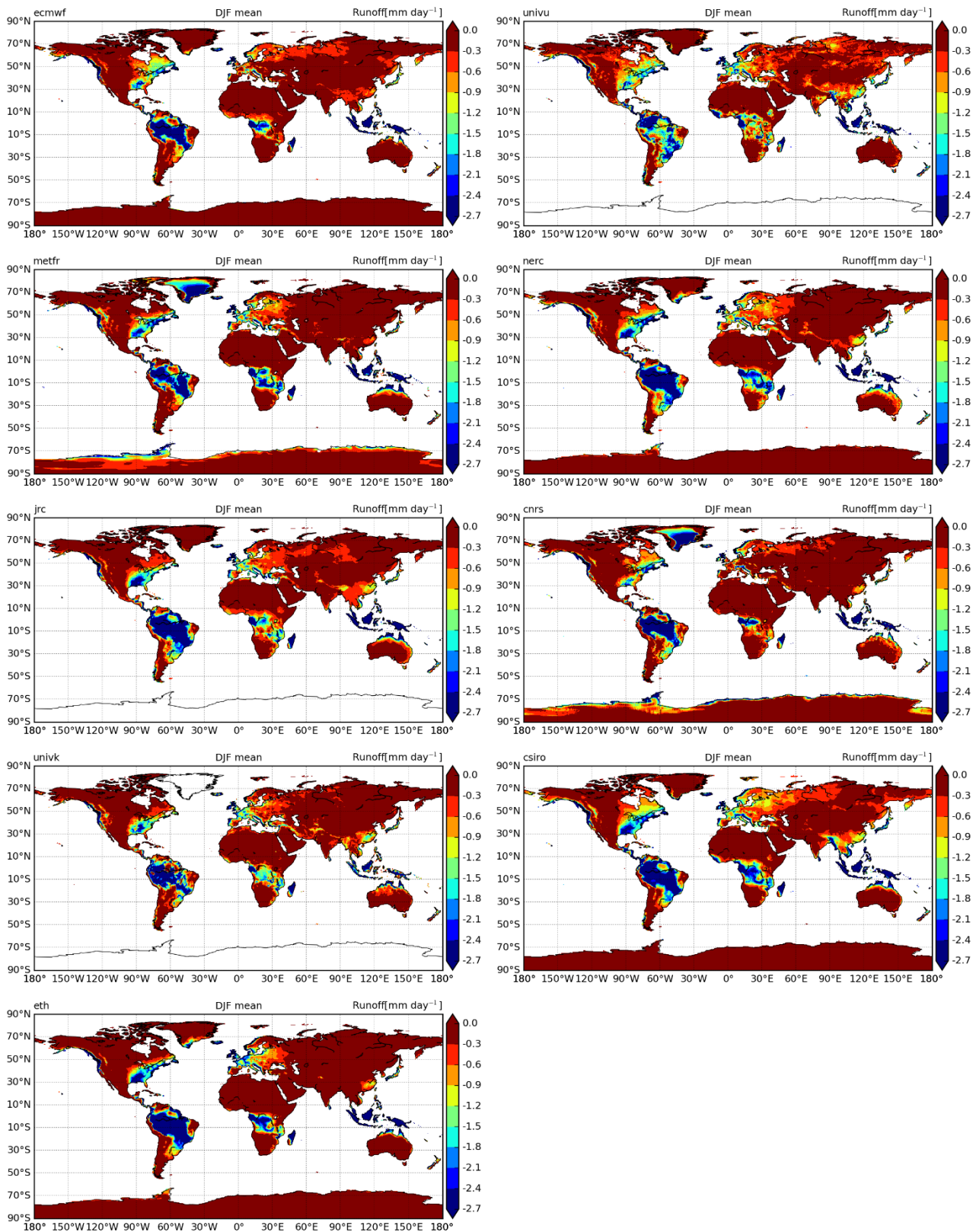


Figure 9.13: Mean northern hemisphere winter runoff in each model.

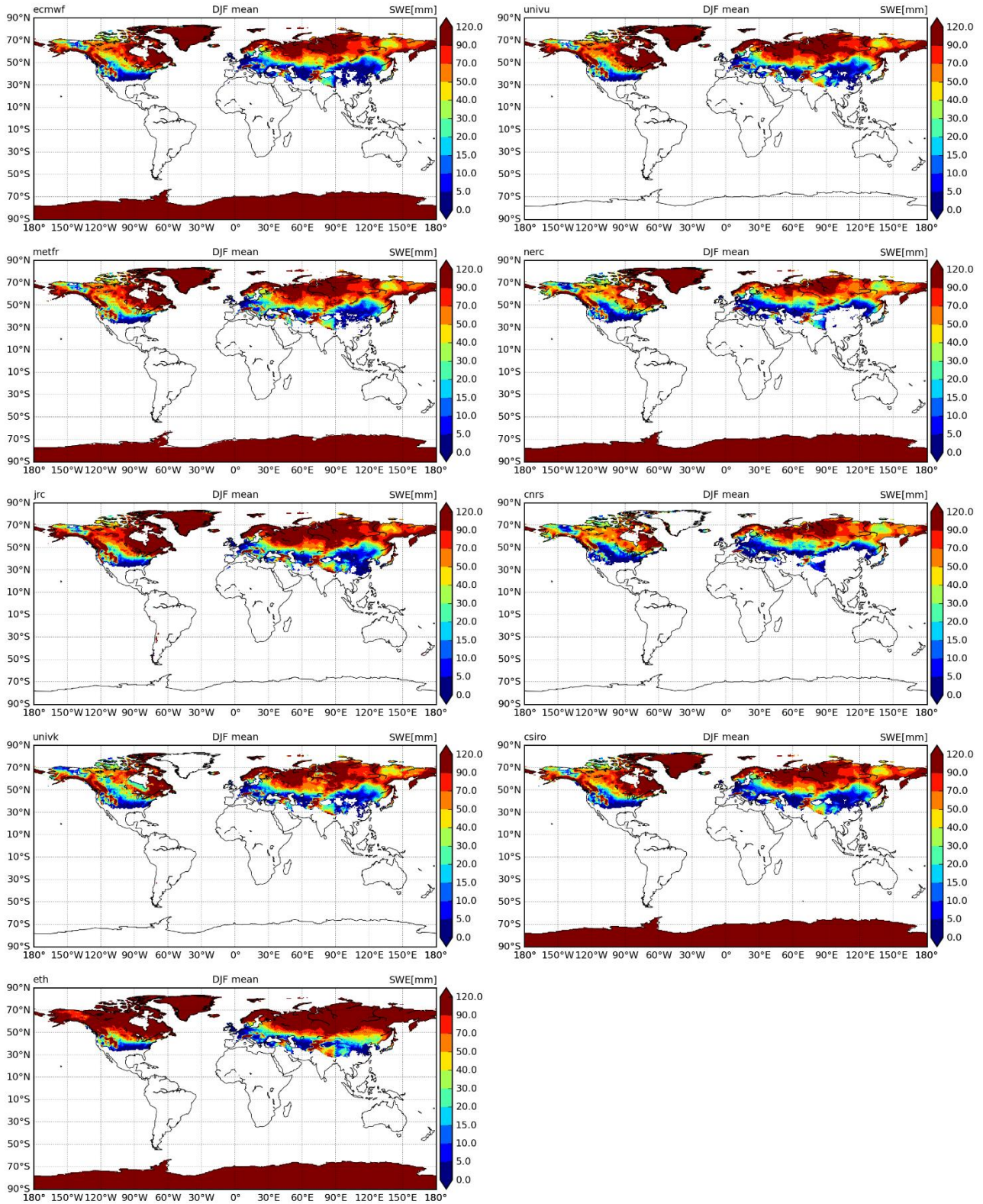


Figure 9.14: Mean northern hemisphere winter SWE in each model.

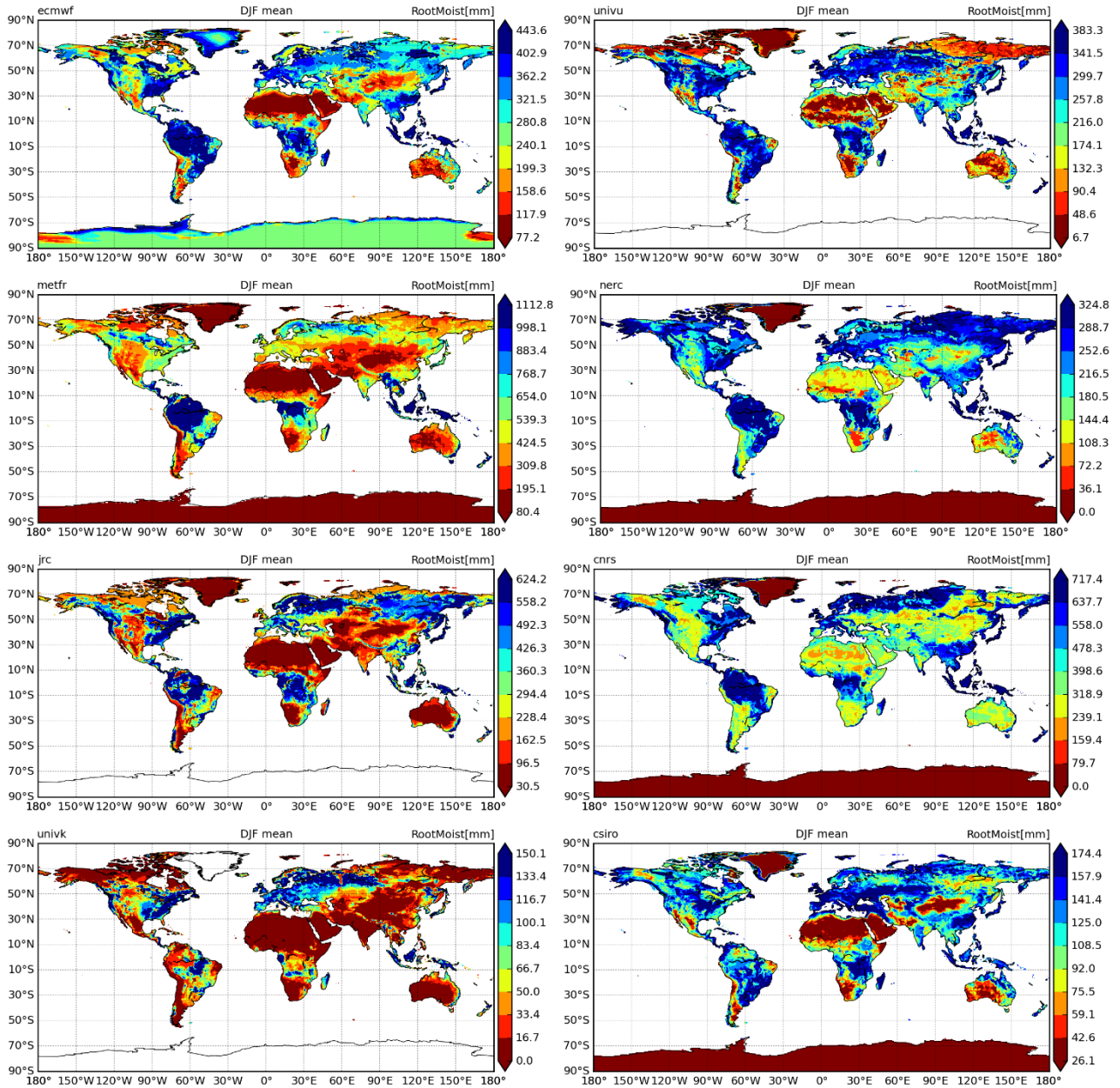


Figure 9.15: Mean northern hemisphere winter RootMoist in each model.

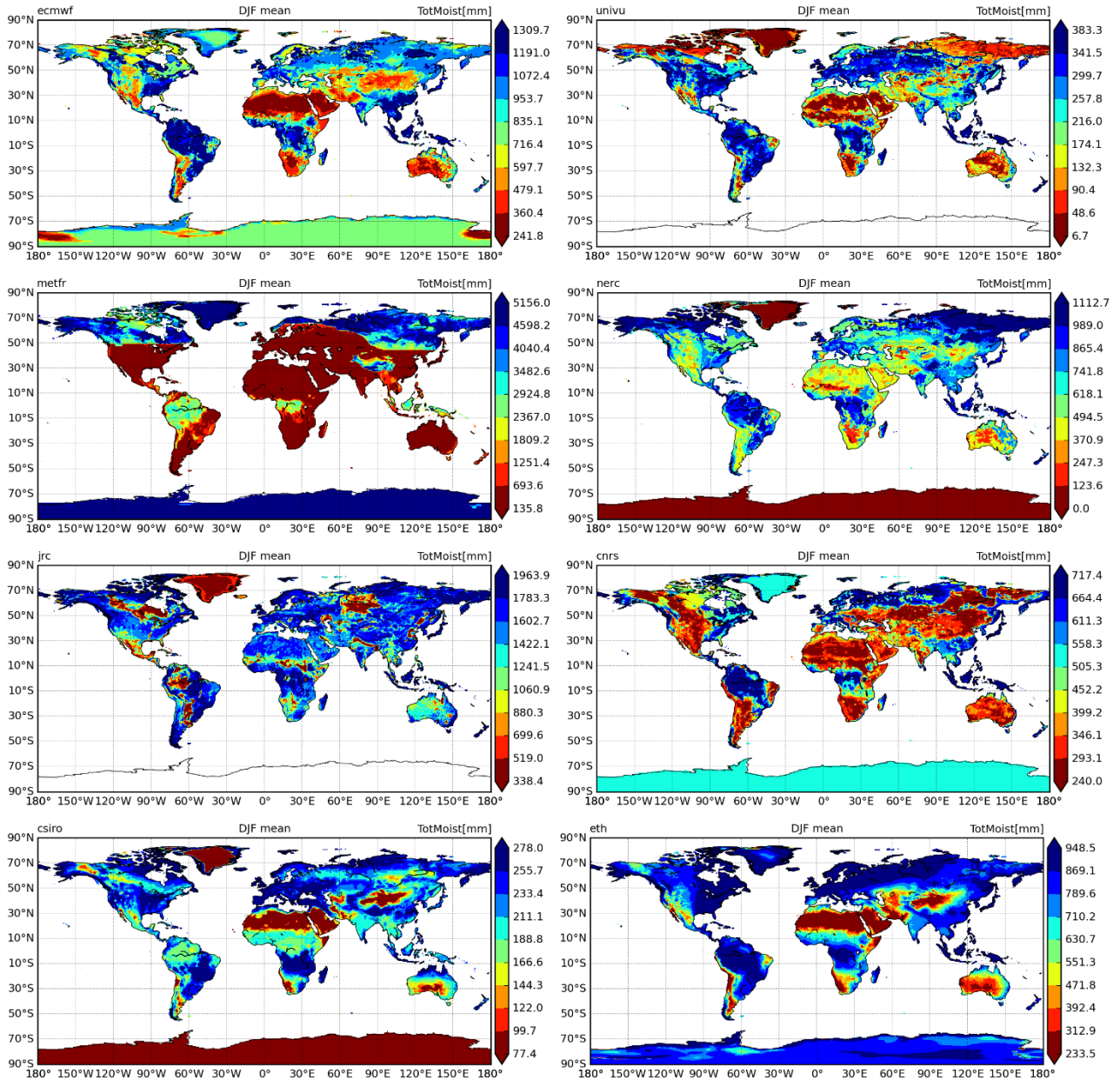


Figure 9.16: Mean northern hemisphere winter TotMoist in each model.

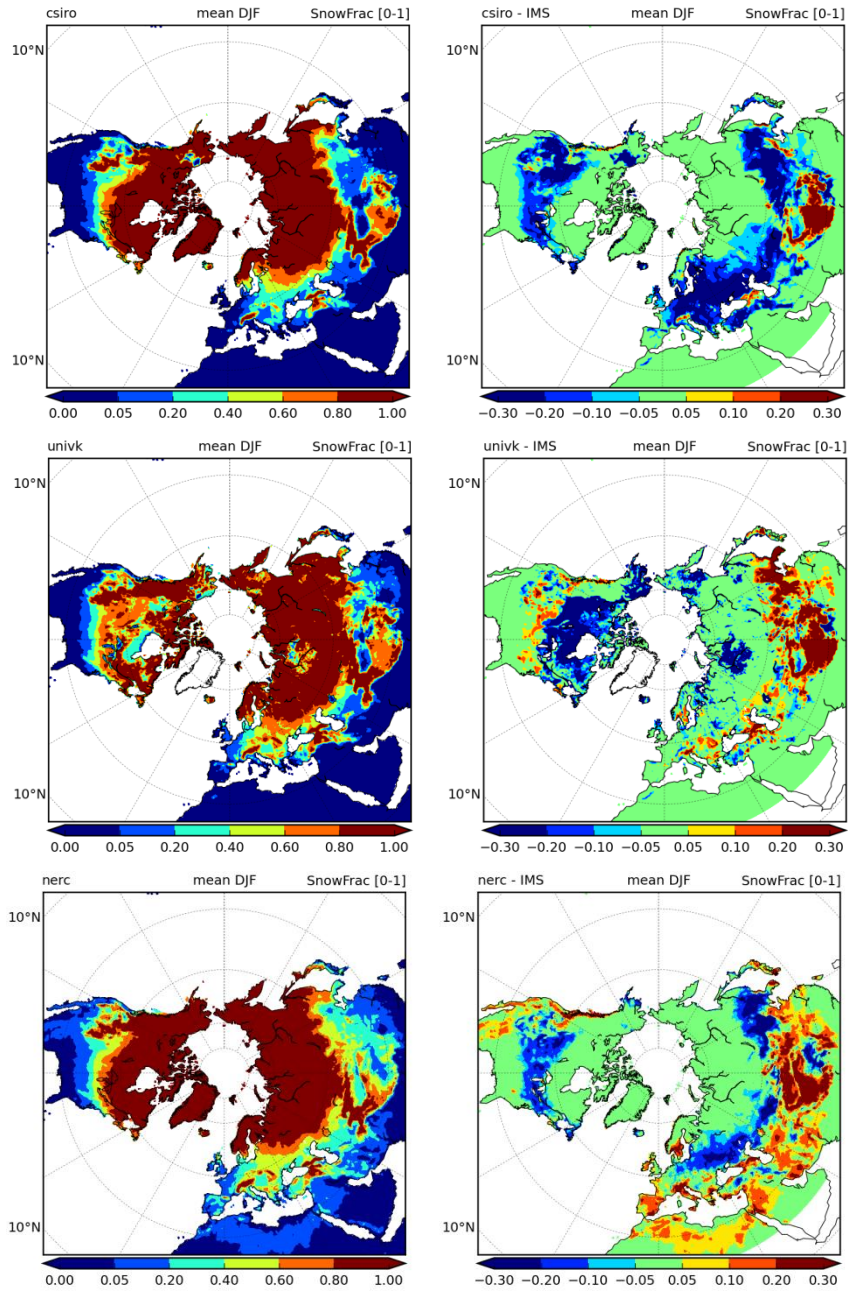


Figure 9.17: Each line contains a specific model mean northern hemisphere winter simulation of snow cover fraction (left) and the mean difference with the IMS dataset (right).

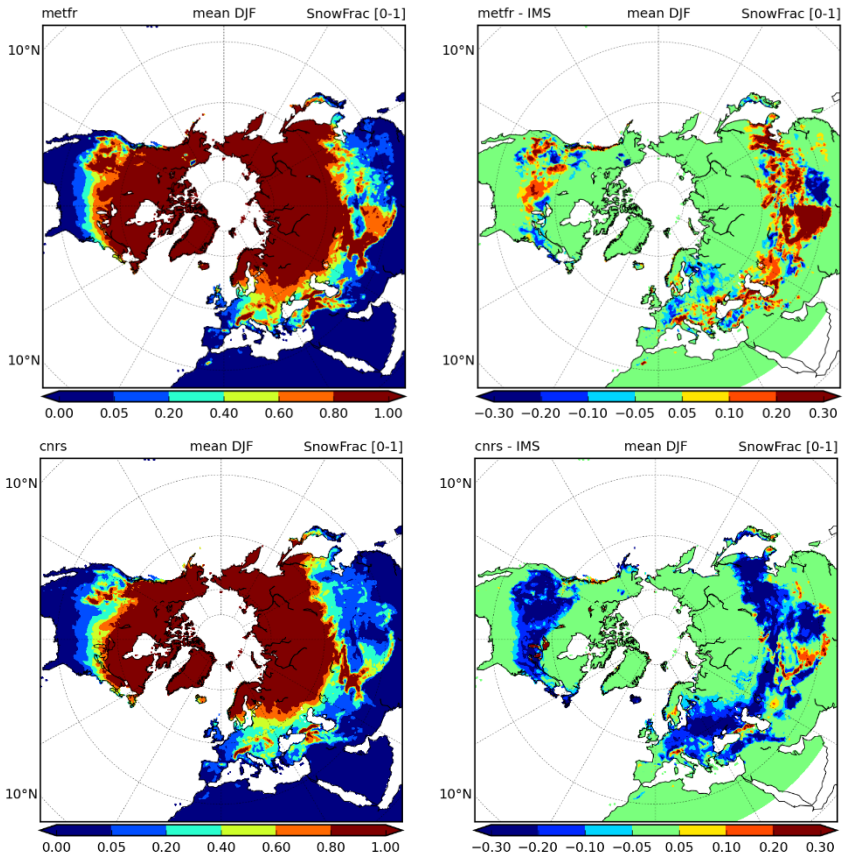


Figure 9.18: As Figure 9.17 for the remaining models.

10 References

- Arrazi, A., Sharon, D., Khain, A., Huss, A., and Mahrer, Y.: THE WINDFIELD AND RAINFALL DISTRIBUTION INDUCED WITHIN A SMALL VALLEY: FIELD OBSERVATIONS AND 2-D NUMERICAL MODELLING, *Boundary Meteorol*, 83, 349-374, doi: 10.1023/a:1000243312103, 1997
- aus der Beek, T., Flörke, M., Lapola, D. M., Schaldach, R., Voß, F., and Teichert, E.: Modelling historical and current irrigation water demand on the continental scale: Europe, *Adv. Geosci.*, 27, 79-85, doi: 10.5194/adgeo-27-79-2010, 2010
- Balsamo, G., Viterbo, P., Beljaars, A., Van den Hurk, B., Betts, A. K., and Scipal, K.: A revised hydrology for the ECMWF model: Verification from field site to terrestrial water storage and impact in the Integrated Forecast System, *J. Hydrometeorol.*, 10, 623-643 doi: 10.1175/2008JHM1068.1171, 2009
- Balsamo, G., Boussetta, S., Dutra, E., Beljaars, A., Viterbo, P., and Van den Hurk, B.: Evolution of land surface processes in the IFS, *ECMWF Newsletter*, 127, 17-22, 2011
- Balsamo, G., Albergel, C., Beljaars, A., Boussetta, S., Brun, E., Cloke, H., Dee, D., Dutra, E., Muñoz-Sabater, J., Pappenberger, F., de Rosnay, P., Stockdale, T., and Vitart, F.: ERA-Interim/Land: a global land surface reanalysis data set, *Hydrol. Earth Syst. Sci.*, 19, 389-407, doi: 10.5194/hess-19-389-2015, 2015
- Barella-Ortiz, A., Polcher, J., Tuzet, A., and Laval, K.: Potential evaporation estimation through an unstressed surface-energy balance and its sensitivity to climate change, *Hydrol. Earth Syst. Sci.*, 17, 4625-4639, doi: 10.5194/hess-17-4625-2013, 2013
- Bergström, S., 1995: The HBV model *Computer models of watershed hydrology*, V. P. Singh, Ed., Water Resources Publications.
- Best, M. J., Pryor, M., Clark, D. B., Rooney, G. G., Essery, R. L. H., Ménard, C. B., Edwards, J. M., Hendry, M. A., Porson, A., Gedney, N., Mercado, L. M., Sitch, S., Blyth, E., Boucher, O., Cox, P. M., Grimmond, C. S. B., and Harding, R. J.: The Joint UK Land Environment Simulator (JULES), model description – Part 1: Energy and water fluxes, *Geosci. Model Dev.*, 4, 677-699, doi: 10.5194/gmd-4-677-2011, 2011
- Beven, K.: Infiltration into a class of vertically non-uniform soils, *Hydrological Sciences Journal*, 29, 425-434, doi: 10.1080/02626668409490960, 1984
- Beven, K., and Germann, P.: Macropores and water flow in soils, *Water Resources Research*, 18, 1311-1325, doi: 10.1029/WR018i005p01311, 1982
- Bontemps, S., Defourny, P., and van Bogaert, E.: GlobCover 2009, products description and validation report., Tech. rep., ESA GlobCover project, available at: <http://ionia1.esrin.esa.int>, 2011
- Brooks, R. H., and Corey, A. T.: Hydraulic properties of porous media, *Hydrological Papers*, 3, Colorado State Univ., Fort Collins, 1964
- Burek, P., Van Der Knijff, J. M., and de Roo, A.: LISFLOOD distributed water balance and flood simulation model revised user manual, Tech. Rep. EUR 26162 EN, Joint Research Centre (JRC), Ispra, Italy, doi: 10.2788/24719, 2013
- Calvet, J.-C., Noilhan, J., Roujean, J.-L., Bessemoulin, P., Cabelguenne, M., Olioso, A., and Wigneron, J.-P.: An interactive vegetation SVAT model tested against data from six contrasting sites, *Agricultural and Forest Meteorology*, 92, 73-95, doi: [http://dx.doi.org/10.1016/S0168-1923\(98\)00091-4](http://dx.doi.org/10.1016/S0168-1923(98)00091-4), 1998
- Cappelaere, B., Vieux, B. E., Peugeot, C., Maia, A., and Séguis, L.: Hydrologic process simulation of a semiarid, endoreic catchment in Sahelian West Niger. 2. Model calibration and uncertainty characterization, *J Hydrol*, 279, 244-261, doi: [http://dx.doi.org/10.1016/S0022-1694\(03\)00182-3](http://dx.doi.org/10.1016/S0022-1694(03)00182-3), 2003
- Cherkauer, K. A., and Lettenmaier, D. P.: Hydrologic effects of frozen soils in the upper Mississippi River basin, *Journal of Geophysical Research: Atmospheres*, 104, 19599-19610, doi: 10.1029/1999jd900337, 1999
- Clapp, R. B., and Hornberger, G. M.: Empirical equations for some soil hydraulic properties, *Water Resources Research*, 14, 601-604, 1978
- Clark, D. B., Mercado, L. M., Sitch, S., Jones, C. D., Gedney, N., Best, M. J., Pryor, M., Rooney, G. G., Essery, R. L. H., Blyth, E., Boucher, O., Harding, R. J., Huntingford, C., and Cox, P. M.: The Joint UK Land Environment Simulator (JULES), model description – Part 2: Carbon fluxes and vegetation dynamics, *Geosci. Model Dev.*, 4, 701-722, doi: 10.5194/gmd-4-701-2011, 2011
- Cox, P. M., Betts, R. A., Bunton, C. B., Essery, R. L. H., Rowntree, P. R., and Smith, J.: The impact of new land surface physics on the GCM simulation of climate and climate sensitivity, *Climate Dyn.*, 15, 183-203, doi: 10.1007/s003820050276, 1999

- D'Orgeval: Impact Du Changement Climatique Sur Le Cycle de L'eau En Afrique de L'Ouest: Modélisation et Incertitudes, PhD Thesis of Université Pierre Marie Curie., 2006
- d'Orgeval, T., Polcher, J., and de Rosnay, P.: Sensitivity of the West African hydrological cycle in ORCHIDEE to infiltration processes, *Hydrol. Earth Syst. Sci.*, 12, 1387-1401, doi: 10.5194/hess-12-1387-2008, 2008
- de Rosnay, P., and Polcher, J.: Modelling root water uptake in a complex land surface scheme coupled to a GCM, *Hydrol. Earth Syst. Sci.*, 2, 239-255, doi: 10.5194/hess-2-239-1998, 1998
- de Rosnay, P., Bruen, M., and Polcher, J.: Sensitivity of surface fluxes to the number of layers in the soil model used in GCMs, *Geophys. Res. Lett.*, 27, 3329-3332, doi: 10.1029/2000gl011574, 2000
- de Rosnay, P., Polcher, J., Bruen, M., and Laval, K.: Impact of a physically based soil water flow and soil-plant interaction representation for modeling large-scale land surface processes, *Journal of Geophysical Research: Atmospheres*, 107, ACL 3-1-ACL 3-19, doi: 10.1029/2001jd000634, 2002
- Decharme, B., Martin, E., and Faroux, S.: Reconciling soil thermal and hydrological lower boundary conditions in land surface models, *Journal of Geophysical Research: Atmospheres*, 118, 7819-7834, doi: 10.1002/jgrd.50631, 2013
- Decharme, B., Boone, A., Delire, C., and Noilhan, J.: Local evaluation of the Interaction between Soil Biosphere Atmosphere soil multilayer diffusion scheme using four pedotransfer functions, *Journal of Geophysical Research: Atmospheres*, 116, D20126, doi: 10.1029/2011jd016002, 2011
- Decharme, B., Douville, H., Boone, A., Habets, F., and Noilhan, J.: Impact of an Exponential Profile of Saturated Hydraulic Conductivity within the ISBA LSM: Simulations over the Rhône Basin, *J. Hydrometeor.*, 7, 61-80, doi: 10.1175/jhm469.1, 2006
- Decharme, B., Alkama, R., Douville, H., Becker, M., and Cazenave, A.: Global Evaluation of the ISBA-TRIP Continental Hydrological System. Part II: Uncertainties in River Routing Simulation Related to Flow Velocity and Groundwater Storage, *J. Hydrometeor.*, 11, 601-617, doi: 10.1175/2010jhm1212.1, 2010
- Dee, D. P., Uppala, S. M., Simmons, A. J., Berrisford, P., Poli, P., Kobayashi, S., Andrae, U., Balmaseda, M. A., Balsamo, G., Bauer, P., Bechtold, P., Beljaars, A. C. M., van de Berg, L., Bidlot, J., Bormann, N., Delsol, C., Dragani, R., Fuentes, M., Geer, A. J., Haimberger, L., Healy, S. B., Hersbach, H., Hólm, E. V., Isaksen, I., Kållberg, P., Köhler, M., Matricardi, M., McNally, A. P., Monge-Sanz, B. M., Morcrette, J. J., Park, B. K., Peubey, C., de Rosnay, P., Tavolato, C., Thépaut, J. N., and Vitart, F.: The ERA-Interim reanalysis: configuration and performance of the data assimilation system, *Quart. J. Roy. Meteor. Soc.*, 137, 553-597, doi: 10.1002/qj.828, 2011
- Dirmeyer, P. A., Gao, X., Zhao, M., Guo, Z., Oki, T., and Hanasaki, N.: GSWP-2: Multimodel Analysis and Implications for Our Perception of the Land Surface, *Bull. Amer. Meteor. Soc.*, 87, 1381-1397, doi: 10.1175/bams-87-10-1381, 2006
- Döll, P., Fiedler, K., and Zhang, J.: Global-scale analysis of river flow alterations due to water withdrawals and reservoirs, *Hydrol. Earth Syst. Sci.*, 13, 2413-2432, doi: 10.5194/hess-13-2413-2009, 2009
- Döll, P., Hoffmann-Dobrev, H., Portmann, F. T., Siebert, S., Eicker, A., Rodell, M., Strassberg, G., and Scanlon, B. R.: Impact of water withdrawals from groundwater and surface water on continental water storage variations, *Journal of Geodynamics*, 59-60, 143-156, doi: <http://dx.doi.org/10.1016/j.jog.2011.05.001>, 2012
- Dutra, E., Balsamo, G., Viterbo, P., Miranda, P. M. A., Beljaars, A., Schar, C., and Elder, K.: An Improved Snow Scheme for the ECMWF Land Surface Model: Description and Offline Validation, *J. Hydrometeor.*, 11, 899-916, doi: 10.1175/2010jhm1249.1, 2010
- Faroux, S., Kaptué Tchuenté, A. T., Roujean, J. L., Masson, V., Martin, E., and Le Moigne, P.: ECOCLIMAP-II/Europe: a twofold database of ecosystems and surface parameters at 1 km resolution based on satellite information for use in land surface, meteorological and climate models, *Geosci. Model Dev.*, 6, 563-582, doi: 10.5194/gmd-6-563-2013, 2013
- Farr, T. G., and Kobrick, M.: Shuttle radar topography mission produces a wealth of data, *Eos, Transactions American Geophysical Union*, 81, 583-585, doi: 10.1029/E0081i048p00583, 2000
- Fekete, B., Vorosmarty, C., and Wolfgang, G.: Global, Composite Runoff Fields Based on Observed River Discharge and Simulated Water Balances, Global Runoff Data Centre, Koblenz, Germany: UNH/GRDC, 2000
- Ferguson, R. I.: Snowmelt runoff models, *Progress in Physical Geography*, 23, 205-227, doi: 10.1177/030913339902300203, 1999
- Flörke, M., Kynast, E., Bärlund, I., Eisner, S., Wimmer, F., and Alcamo, J.: Domestic and industrial water uses of the past 60 years as a mirror of socio-economic development: A global simulation study, *Global Environmental Change*, 23, 144-156, doi: <http://dx.doi.org/10.1016/j.gloenvcha.2012.10.018>, 2013
- Gleeson, T., Smith, L., Moosdorf, N., Hartmann, J., Dürr, H. H., Manning, A. H., van Beek, L. P. H., and Jellinek, A. M.: Mapping permeability over the surface of the Earth, *Geophys. Res. Lett.*, 38, L02401, doi: 10.1029/2010gl045565, 2011

- Gong, L., Halldin, S., and Xu, C. Y.: Global-scale river routing—an efficient time-delay algorithm based on HydroSHEDS high-resolution hydrography, *Hydrol. Processes*, 25, 1114-1128, doi: 10.1002/hyp.7795, 2011
- Goutorbe, J. P., Lebel, T., Tinga, A., Bessemoulin, P., Brouwer, J., Dolman, A. J., Engman, E. T., Gash, J. H. C., Hoepffner, M., Kabat, P., Kerr, Y. H., Monteny, B., Prince, S., Said, F., Sellers, P., and Wallace, J. S.: HAPEX-Sahel: a large-scale study of land-atmosphere interactions in the semi-arid tropics, *Ann. Geophys.*, 12, 53-64, doi: 10.1007/s00585-994-0053-0, 0001
- Hagemann, S., and Dümenil, L.: A parametrization of the lateral waterflow for the global scale, *Climate Dyn.*, 14, 17-31, doi: 10.1007/s003820050205, 1997
- Hagemann, S., and Gates, L. D.: Improving a subgrid runoff parameterization scheme for climate models by the use of high resolution data derived from satellite observations, *Climate Dyn.*, 21, 349-359, doi: 10.1007/s00382-003-0349-x, 2003
- Hamon, W. R.: Estimating Potential Evapotranspiration, *J. Hydraulics Div., Proc. Am. Soc. Civ. Eng.*, 87, 107-120, 1961
- Hansen, M. C., DeFries, R. S., Townshend, J. R. G., Carroll, M., Dimiceli, C., and Sohlberg, R. A.: Global Percent Tree Cover at a Spatial Resolution of 500 Meters: First Results of the MODIS Vegetation Continuous Fields Algorithm, *Earth Interactions*, 7, 1-15, doi: 10.1175/1087-3562(2003)007<0001:gptcaa>2.0.co;2, 2003
- Harding, R., Best, M., Blyth, E., Hagemann, S., Kabat, P., Tallaksen, L. M., Warnaars, T., Wiberg, D., Weedon, G. P., Lanen, H. v., Ludwig, F., and Haddeland, I.: WATCH: Current Knowledge of the Terrestrial Global Water Cycle, *J. Hydrometeor.*, 12, 1149-1156, doi: 10.1175/jhm-d-11-024.1, 2011
- Hengl, T., de Jesus, J., MacMillan, R., and Heuvelink, G.: SoilGrids1km — Global Soil Information Based on Automated Mapping, *PLoS ONE*, 9, e105992, doi: 10.1371/journal.pone.0105992, 2014
- Iizumi, T., Okada, M., and Yokozawa, M.: A meteorological forcing data set for global crop modeling: Development, evaluation, and intercomparison, *Journal of Geophysical Research: Atmospheres*, 119, 2013JD020130, doi: 10.1002/2013jd020130, 2014
- Jarvis, A., Reuter, H. I., Nelson, A., and Guevera, E., cited 2006: Hole-filled SRTM for the Globe Version 4. [Available online at <http://srtm.csi.cgiar.org>.]
- Koster, R. D., and P. Mahanama, S. P.: Land Surface Controls on Hydroclimatic Means and Variability, *J. Hydrometeor.*, 13, 1604-1620, doi: 10.1175/jhm-d-12-050.1, 2012
- Kraaijenhoff van de Leur, D.: A study of non-steady groundwater flow with special reference to a reservoir coefficient, *De Ingenieur*, 70, 87-94, 1958
- Lehner, B., and Doll, P.: Development and validation of a global database of lakes, reservoirs and wetlands, *J Hydrol*, 296, 1-22, 2004
- Lehner, B., Liermann, C. R., Revenga, C., Vörösmarty, C., Fekete, B., Crouzet, P., Döll, P., Endejan, M., Frenken, K., Magome, J., Nilsson, C., Robertson, J. C., Rödel, R., Sindorf, N., and Wissler, D.: High-resolution mapping of the world's reservoirs and dams for sustainable river-flow management, *Frontiers in Ecology and the Environment*, 9, 494-502, doi: 10.1890/100125, 2011
- Lindström, G., Johansson, B., Persson, M., Gardelin, M., and Bergström, S.: Development and test of the distributed HBV-96 hydrological model, *J Hydrol*, 201, 272-288, doi: [http://dx.doi.org/10.1016/S0022-1694\(97\)00041-3](http://dx.doi.org/10.1016/S0022-1694(97)00041-3), 1997
- Loveland, T. R., Reed, B. C., Brown, J. F., Ohlen, D. O., Zhu, Z., Yang, L., and Merchant, J. W.: Development of a global land cover characteristics database and IGBP DISCover from 1 km AVHRR data, *Int. J. Remote Sens.*, 21, 1303-1330, 2000
- Masson, V., Le Moigne, P., Martin, E., Faroux, S., Alias, A., Alkama, R., Belamari, S., Barbu, A., Boone, A., Bouyssel, F., Brousseau, P., Brun, E., Calvet, J. C., Carrer, D., Decharme, B., Delire, C., Donier, S., Essaouini, K., Gibelin, A. L., Giordani, H., Habets, F., Jidane, M., Kerdraon, G., Kourzeneva, E., Lafaysse, M., Lafont, S., Lebeaupin Brossier, C., Lemonsu, A., Mahfouf, J. F., Marguinaud, P., Mokhtari, M., Morin, S., Pigeon, G., Salgado, R., Seity, Y., Taillefer, F., Tanguy, G., Tulet, P., Vincendon, B., Vionnet, V., and Voldoire, A.: The SURFEXv7.2 land and ocean surface platform for coupled or offline simulation of earth surface variables and fluxes, *Geosci. Model Dev.*, 6, 929-960, doi: 10.5194/gmd-6-929-2013, 2013
- Miller, J. R., Russell, G. L., and Caliri, G.: Continental-Scale River Flow in Climate Models, *J. Climate*, 7, 914-928, doi: 10.1175/1520-0442(1994)007<0914:csrffc>2.0.co;2, 1994
- Monsi, M., and Saeki, T.: Über den Lichtfaktor in den Pflanzengesellschaften und seine Bedeutung für die Stoffproduktion, *Japanese Journal of Botany*, 14, 22-52, doi: citeulike-article-id:1687877, 1953
- Moody, E. G., King, M. D., Platnick, S., Schaaf, C. B., and Feng, G.: Spatially complete global spectral surface albedos: value-added datasets derived from Terra MODIS land products, *Geoscience and Remote Sensing, IEEE Transactions on*, 43, 144-158, doi: 10.1109/tgrs.2004.838359, 2005

- Moore, R. J.: The probability-distributed principle and runoff production at point and basin scales *Hydrological Sciences Journal*, 30, 273-297, 1985
- Muller, J. P., Lopez, G. L., Watson, D. J., Shane, N., Kennedy, T., Yuen, P., and Lewis, P.: The ESA GlobAlbedo project for mapping the Earth's land surface albedo for 15 years from European sensors, *Geophysical Research Abstracts*, 13 (EGU2011-10969). 2011
- Mulligan, M.: WaterWorld: a self-parameterising, physically based model for application in data-poor but problem-rich environments globally, *Hydrology Research*, 44, 748-769, doi: doi:10.2166/nh.2012.217, 2013
- Mulligan, M., and Burke, S. M.: FIESTA: Fog Interception for the Enhancement of Streamflow in Tropical Areas, <http://www.ambiotek.com/fiesta>, 174pp, 2005
- Oki, T., and Sud, Y. C.: Design of Total Runoff Integrating Pathways (TRIP)—A Global River Channel Network, *Earth Interactions*, 2, 1-37, doi: 10.1175/1087-3562(1998)002<0001:dotrip>2.3.co;2, 1998
- Oki, T., Agata, Y., Kanae, S., Saruhashi, T., Yang, D., and Musiak, K.: Global assessment of current water resources using total runoff integrating pathways, *Hydrological Sciences Journal*, 46, 983-995, doi: 10.1080/02626660109492890, 2001
- Orth, R., and Seneviratne, S. I.: Predictability of soil moisture and streamflow on subseasonal timescales: A case study, *Journal of Geophysical Research: Atmospheres*, 118, 10,963-910,979, doi: 10.1002/jgrd.50846, 2013
- Orth, R., and Seneviratne, S.: Using soil moisture forecasts for sub-seasonal summer temperature predictions in Europe, *Climate Dyn.*, 43, 3403-3418, doi: 10.1007/s00382-014-2112-x, 2014
- Orth, R., and Seneviratne, S.: Introduction of a simple-model-based land surface dataset for Europe, submitted to *Env. Res. Lett.*, 2015
- Peeters, L. J. M., Crosbie, R. S., Doble, R. C., and Van Dijk, A. I. J. M.: Conceptual evaluation of continental land-surface model behaviour, *Environmental Modelling & Software*, 43, 49-59, doi: <http://dx.doi.org/10.1016/j.envsoft.2013.01.007>, 2013
- Peña-Arancibia, J. L., van Dijk, A. I. J. M., Mulligan, M., and Bruijnzeel, L. A.: The role of climatic and terrain attributes in estimating baseflow recession in tropical catchments, *Hydrol. Earth Syst. Sci.*, 14, 2193-2205, doi: 10.5194/hess-14-2193-2010, 2010
- Peugeot, C., Cappelaere, B., Vieux, B. E., Séguis, L., and Maia, A.: Hydrologic process simulation of a semiarid, endoreic catchment in Sahelian West Niger. 1. Model-aided data analysis and screening, *J Hydrol*, 279, 224-243, doi: [http://dx.doi.org/10.1016/S0022-1694\(03\)00181-1](http://dx.doi.org/10.1016/S0022-1694(03)00181-1), 2003
- Prigent, C., Papa, F., Aires, F., Rossow, W. B., and Matthews, E.: Global inundation dynamics inferred from multiple satellite observations, 1993–2000, *J. Geophys. Res.*, 112, D12107, doi: 10.1029/2006jd007847, 2007
- Reynolds, C. A., Jackson, T. J., and Rawls, W. J.: Estimating soil water-holding capacities by linking the Food and Agriculture Organization Soil map of the world with global pedon databases and continuous pedotransfer functions, *Water Resources Research*, 36, 3653-3662, doi: 10.1029/2000wr900130, 2000
- Supit, I., Hooijer, A. A., and Van Diepen, C. A., 1994: Volume 1: Theory and Algorithms. *System Description of the WOFOST 6.0 Crop Simulation Model Implemented in CGMS*, I. Supit, A. A. Hooijer, and C. A. Van Diepen, Eds., Office for Official Publications of the European Communities.
- Sutanudjaja, E. H., Van Beek, L. P. H., Wada, Y., Wisser, D., Graaf, I. E. M., Straatsma, M. W., and Bierkens, M. F. P., 2014: Development and validation of PCR-GLOBWB 2.): a 5 arc min resolution global hydrology and water resources model. *EGU*, Vienna, Austria.
- Todini, E.: The ARNO rainfall—runoff model, *J Hydrol*, 175, 339-382, doi: [http://dx.doi.org/10.1016/S0022-1694\(96\)80016-3](http://dx.doi.org/10.1016/S0022-1694(96)80016-3), 1996
- USGS EROS Data Center: Global land cover characteristics data base version 2.0, http://edc2.usgs.gov/glcc/globe_int.php, 2002
- : HYDRO1k Elevation Derivative Database, <https://lta.cr.usgs.gov/GTOPO30> 2006
- van Beek, L. P. H., Wada, Y., and Bierkens, M. F. P.: Global monthly water stress: 1. Water balance and water availability, *Water Resources Research*, 47, W07517, doi: 10.1029/2010wr009791, 2011
- Van Der Knijff, J. M., Younis, J., and De Roo, A. P. J.: LISFLOOD: a GIS-based distributed model for river basin scale water balance and flood simulation, *International Journal of Geographical Information Science*, 24, 189-212, doi: 10.1080/13658810802549154, 2008
- Van Deursen, W. P. A., 1995: *Geographical information systems and dynamic models: development and application of a prototype spatial modelling language*.
- van Dijk, A. I. J. M.: Climate and terrain factors explaining streamflow response and recession in Australian catchments, *Hydrol. Earth Syst. Sci.*, 14, 159-169, doi: 10.5194/hess-14-159-2010, 2010a

- Van Dijk, A. I. J. M.: AWRA Technical Report 3, Landscape Model (Version 0.5) Technical Description, WIRADA/CSIRO Water for a Healthy Country Flagship, Canberra, [Available at <http://www.clw.csiro.au/publications/waterforahealthycountry/2010/wfhc-aus-water-resources-assessment-system.pdf>.] 2010b
- van Dijk, A. I. J. M.: Selection of an appropriately simple storm runoff model, *Hydrol. Earth Syst. Sci.*, 14, 447-458, doi: 10.5194/hess-14-447-2010, 2010c
- van Dijk, A. I. J. M., and Bruijnzeel, L. A.: Modelling rainfall interception by vegetation of variable density using an adapted analytical model. Part 1. Model description, *J Hydrol*, 247, 230-238, doi: [http://dx.doi.org/10.1016/S0022-1694\(01\)00392-4](http://dx.doi.org/10.1016/S0022-1694(01)00392-4), 2001
- van Dijk, A. I. J. M., and Renzullo, L. J.: Water resource monitoring systems and the role of satellite observations, *Hydrol. Earth Syst. Sci.*, 15, 39-55, doi: 10.5194/hess-15-39-2011, 2011
- van Dijk, A. I. J. M., Peña-Arancibia, J. L., Wood, E. F., Sheffield, J., and Beck, H. E.: Global analysis of seasonal streamflow predictability using an ensemble prediction system and observations from 6192 small catchments worldwide, *Water Resources Research*, 49, 2729-2746, doi: 10.1002/wrcr.20251, 2013
- van Genuchten, M. T.: A Closed Form Equation for Predicting the Hydraulic Conductivity of Unsaturated Soils, *Soil Sci Soc Am J*, 44, 892-898, 1980
- Verzano, K.: Climate change impacts on flood related hydrological processes: Further development and application of a global scale hydrological model, *Reports on Earth System Science*, 71, Max Planck Institute for Meteorology, Hamburg, Germany, 2009
- Verzano, K., Bärlund, I., Flörke, M., Lehner, B., Kynast, E., Voß, F., and Alcamo, J.: Modeling variable river flow velocity on continental scale: Current situation and climate change impacts in Europe, *J Hydrol*, 424-425, 238-251, doi: <http://dx.doi.org/10.1016/j.jhydrol.2012.01.005>, 2012
- Viterbo, P., Beljaars, A., Mahfouf, J. F., and Teixeira, J.: The representation of soil moisture freezing and its impact on the stable boundary layer, *Quart. J. Roy. Meteor. Soc.*, 125, 2401-2426, doi: 10.1002/qj.49712555904, 1999
- Vörösmarty, C., and Moore, B., III: Modeling basin-scale hydrology in support of physical climate and global biogeochemical studies: An example using the Zambezi River, *Surv Geophys*, 12, 271-311, doi: 10.1007/bf01903422, 1991
- Weedon, G. P., Balsamo, G., Bellouin, N., Gomes, S., Best, M. J., and Viterbo, P.: The WFDEI meteorological forcing data set: WATCH Forcing Data methodology applied to ERA-Interim reanalysis data, *Water Resources Research*, 50, 7505-7514, doi: 10.1002/2014wr015638, 2014
- Yamazaki, D., Oki, T., and Kanae, S.: Deriving a global river network map and its sub-grid topographic characteristics from a fine-resolution flow direction map, *Hydrol. Earth Syst. Sci.*, 13, 2241-2251, doi: 10.5194/hess-13-2241-2009, 2009
- Yamazaki, D., Kanae, S., Kim, H., and Oki, T.: A physically based description of floodplain inundation dynamics in a global river routing model, *Water Resour. Res.*, 47, W04501, doi: 10.1029/2010wr009726, 2011
- Yebra, M., Van Dijk, A., Leuning, R., Huete, A., and Guerschman, J. P.: Evaluation of optical remote sensing to estimate actual evapotranspiration and canopy conductance, *Remote Sens. Environ.*, 129, 250-261, doi: <http://dx.doi.org/10.1016/j.rse.2012.11.004>, 2013
- Yu, Z.: Assessing the response of subgrid hydrologic processes to atmospheric forcing with a hydrologic model system, *Global Planet. Change*, 25, 1-17, doi: [http://dx.doi.org/10.1016/S0921-8181\(00\)00018-7](http://dx.doi.org/10.1016/S0921-8181(00)00018-7), 2000